Identifying *in vivo* genetic dependencies of melanocyte and melanoma development

Sarah Perlee[1,2], Yilun Ma[1,3,4], Miranda V. Hunter[1], Jacob B. Swanson[5,6], Nelly M. Cruz[1], Zhitao Ming[7], Julia Xia[1], Timothée Lionnet[5,6,8], Maura McGrail[7], Richard M. White[1,9,*]

[1]Department of Cancer Biology and Genetics, Memorial Sloan Kettering Cancer Center, New York, NY, USA
[2]Gerstner Sloan Kettering Graduate School of Biomedical Sciences, Memorial Sloan Kettering Cancer Center, New York, NY, USA.
[3]Weill Cornell/Rockefeller/Sloan Kettering Tri-Institutional MD-PhD Program, Memorial Sloan Kettering Cancer Center, New York, NY, USA.
[4]Cell and Developmental Biology Program, Weill Cornell Graduate School of Medical Sciences, New York, NY, USA.
[5]Institute for Systems Genetics, NYU Grossman School of Medicine, New York, NY, USA.
[6]Department of Cell Biology, NYU Grossman School of Medicine, New York, NY, USA.
[7]Department of Genetics, Development and Cell Biology, Iowa State University, IA, USA.
[8]Department of Biomedical Engineering, NYU Tandon School of Engineering, Brooklyn, NY.
[9]Nuffield Department of Medicine, Ludwig Institute for Cancer Research, University of Oxford, Oxford, UK.
[*] Correspondence to Richard M. White: Richard.white@ludwig.ox.ac.uk

Abstract

The advent of large-scale sequencing in both development and disease has identified large numbers of candidate genes that may be linked to important phenotypes. We have developed a rapid, scalable system for assessing the role of candidate genes using zebrafish. We generated transgenic zebrafish in which Cas9 was knocked-in to the endogenous *mitfa* locus, a master transcription factor of the melanocyte lineage. The main advantage of this system compared to existing techniques is maintenance of endogenous regulatory elements. We used this system to identify both cell-autonomous and non-cell autonomous regulators of normal melanocyte development. We then applied this to the melanoma setting to demonstrate that loss of genes required for melanocyte survival can paradoxically promote more aggressive phenotypes, highlighting that *in vitro* screens can mask *in vivo* phenotypes. Our genetic approach offers a versatile tool for exploring developmental processes and disease mechanisms that can readily be applied to other cell lineages.

Introduction:

Cell type-specific knockout of genes is crucial for unraveling the intricate molecular mechanisms underlying cell function, development, and transformation. Efficient methods are critical as sequencing projects such as All of Us, the UK Biobank and the Cancer DepMap continue to identify hundreds of new candidate genes on a regular

basis, many of which have yet to be characterized *in vivo*[1-3]. Zebrafish (*Danio rerio*) have emerged as a powerful genetic model organism for studying these processes. The large number of animals that can be easily generated make it advantageous (compared to other systems like mice) for querying large numbers of genetic variants that may have links to human diseases. However, most studies in this system use germline knockout, which makes it difficult to determine whether the identified gene has a specific function in a particular lineage, or whether the phenotype reflects a more general developmental defect. Furthermore, many genes which might have lineage specific functions cannot be studied using germline knockout, since embryonic lethality often accompanies global knockout of essential genes[4]. To overcome these limitations, several groups have explored tissue-specific and conditional knockout strategies in zebrafish[5-13]. For example, the MAZERATI system uses tissue-specific promoter transgenes to drive Cas9 expression, which are introduced via plasmid injection into one-cell stage embryos[6,14]. This system has been shown to be versatile and powerful. One potential limitation of promoter fragment transgenes is that these fragments could lack certain regulatory regions. For this reason, it is common in systems such as mice to knock in genetic cassettes (i.e. Cre recombinase) into endogenous loci.

In this study, we wished to develop such an endogenous system to understand *in vivo* genetic dependencies, using melanocytes and melanoma as an exemplar. Skin color pigmentation is amongst the most heterogeneous of genetic systems, with a large number of loci linked to melanocyte development. Mutations in pleiomorphic genes such as *sox10, ednrb, jam3b, tuba8l3, meox1* and *kit* yield clear defects in melanocyte/melanophore development, but these mutants also have defects in other tissues[15-21]. Many of these genes are also expressed in melanoma, but their specific *in vivo* function in tumorigenesis remains poorly understood. By integrating the Cas9 nuclease into the endogenous melanocyte-specific *mitfa* locus, we achieved specific gene disruption across the melanocyte developmental lineage. We used our *mitfa*^{Cas9} knockin animals to inactivate the pigmentation gene *albino* and the embryonic essential genes *sox10, tuba1a,* and *ptena/b* in melanocytes without additional developmental or off-target phenotypes. We also demonstrated that this system can be used to induce melanomas in wild-type fish by inactivating the tumor suppressors *tp53* and *ptena/b* within melanocytes also expressing the melanoma oncogene BRAF^{V600E}. Inactivating the neural crest transcription factor *sox10* in these tumors significantly decreased melanoma initiation but resulted in rare invasive tumors that highly expressed the *sox9* transcription factor, highlighting that unexpected *in vivo* phenotypes can emerge that aren't predicted from *in vitro* studies[22,23]. Our system can thus be used to advance our understanding of melanocyte biology and the genetic underpinnings of phenotypic switching in melanoma, an approach that can readily be used for other cell types.

Results:

Targeted integration of Cas9 to the *mitfa* locus

To selectively disrupt genes in a melanocyte lineage-specific manner while retaining natural regulatory elements, we established a transgenic zebrafish line harboring Cas9 at the endogenous *mitfa* locus. *Mitfa* expression is detectable by 18 hours postfertilization (hpf) and is highly expressed in pigment cells including melanocytes,

xanthophores and their progenitors. To achieve knock-in, we utilized the GeneWeld method, which enables efficient integration of DNA cassettes using homology mediated end joining (HMEJ)[24,25]. The knock-in cassette, containing Cas9 and BFP driven by the eye-specific γ-crystallin promoter, was targeted to exon 2 of the *mitfa* gene, which leads to disruption of the endogenous *mitfa* gene (Figure 1A). We strategically selected this genomic site for several reasons. First, this is the sole exon shared among the three *mitfa* protein-coding transcripts. Furthermore, targeting Cas9 to exon 2 offers the flexibility of replicating this knock-in strategy in *casper* zebrafish, a transparent fish widely used for melanoma studies that harbor a premature stop codon in *mitfa* exon 3[26].

The knock-in vector, along with Cas9 protein and guide RNAs targeting either the *mitfa* integration site or the sequences flanking the 5' and 3' homology arms, were injected into 1-cell stage wild-type Tropical 5D (T5D) zebrafish embryos (Figure 1B)[27]. An average of 19% of injected embryos had detectable ocular BFP expression at 3 days postfertilization (dpf), indicating successful integration (Figure S1A). Embryos were raised to adulthood then crossed with WT T5D fish. The resulting F1 embryos were screened for BFP+ eyes and tail clippings were sequenced to confirm precise integration of the knock-in cassette at the *mitfa* locus. We sequenced four F1 fish and detected on-target integration at the *mitfa* locus in all four fish (Figure S1B). In zebrafish, one copy of *mitfa* is sufficient for the normal development of neural crest-derived melanocytes, but loss of both copies of *mitfa* results in loss of the melanocyte lineage[26,28]. To determine the effect of a single copy of *mitfa*^{Cas9} on melanocytes, *mitfa*^{Cas9} fish were in-crossed and the resulting siblings were imaged at various time points (Figure S1C). WT and *mitfa*^{Cas9} fish exhibited indistinguishable melanocyte patterning during both embryonic and adult stages. However, as expected, fish carrying two copies of Cas9 (*mitfa*$^{Cas9/Cas9}$) resembled the *nacre* mutant (*mitfa*-/-), characterized by complete loss of melanocytes, indicating the endogenous *mitfa* gene is disrupted on knock-in alleles[28]. We used zebrafish harboring one knock-in allele (*mitfa*^{Cas9}) for all subsequent experiments to allow us to test gene function in melanocytes.

To determine whether Cas9 expression was restricted to melanocytes, we performed fluorescence in situ hybridization (FISH) on 3dpf WT and *mitfa*^{Cas9} embryos to assess *mitfa* and Cas9 mRNA expression (Figure 1C and S1D). As expected, *mitfa* was detected within the embryonic melanocyte stripe regions in both WT and *mitfa*^{Cas9} fish. In *mitfa*^{Cas9} embryos, Cas9 expression was observed in an average of 86% of these *mitfa*+ cells (Figure S1D). These results provide functional validation for on-target integration and melanocyte lineage-restricted expression of Cas9.

Melanocyte-specific loss of the human skin color associated gene *slc45a2* results in robust loss of pigmentation

To assess the effectiveness of our stable *mitfa*^{Cas9} line, we first targeted the *albino* gene (*slc45a2*). Large scale GWAS studies have repeatedly identified SNPs in this gene as tightly linked to human skin color variation, and germline disruption leads to a complete loss of pigmentation in melanocytes[29-31]. This distinct phenotype enables the visual observation of Cas9 activity in zebrafish injected with *albino* gRNA. To test our system, we designed plasmids, denoted MG-gRNA, containing a zU6:gRNA cassette followed

139 by *mitfa*:GFP to enable visualization of cells expressing the *albino* gRNA. MG-*albino*
140 and MG-NT were injected into one-cell stage embryos from crosses between *mitfa*^{Cas9}
141 and WT fish, which express Cas9 in all melanocytes but exhibit mosaic gRNA
142 expression (Figure 2A).
143
144 Embryos were screened for BFP+ eyes to identify those harboring *mitfa*^{Cas9}. Upon
145 adulthood, 92% of F0 MG-*albino* fish had mosaic loss of pigmentation within the
146 melanocyte stripe regions (Figure 2B-C). Unpigmented regions maintained GFP
147 expression (Figure 2B), indicating that the breaks in melanocyte stripes arise from loss
148 of pigmentation in melanocytes rather than loss of the melanocyte lineage (Figure 2B).
149 As expected, control MG-NT clutch mates displayed normal pigmentation and GFP+
150 melanocytes were indistinguishable from GFP- regions on the same fish (Figure 2B-C).
151
152 We next aimed to determine the efficiency of *mitfa*^{Cas9} in the F1 generation, in which
153 every melanocyte stably expresses the *albino* gRNA and *mitfa*^{Cas9}. To generate F1
154 lines, we outcrossed the F0 MG-gRNA fish to WT and sorted embryos for BFP+ eyes
155 and GFP+ melanocytes. F1 MG-*albino* fish exhibited a near complete loss of
156 pigmentation, demonstrating that our *mitfa*^{Cas9} system is highly efficient in F1 fish
157 (Figure 2D-E). To study the effect of *albino* inactivation across various stages of
158 development, F1 MG-gRNA fish were once again outcrossed to WT, generating F2 MG-
159 gRNA fish expressing one copy of *mitfa*^{Cas9}. Imaging revealed a measurable
160 pigmentation loss in F2 MG-*albino* melanocytes as early as 3 days post-fertilization
161 (dpf) (Figure 2F-G). F2 MG-*albino* fish maintained loss of pigmentation throughout
162 development, indicating the sustained activity of *mitfa*^{Cas9} (Figure S2A-D).
163
164 To confirm on-target cutting of the *albino* gene in the melanocyte lineage (and not other
165 tissues), the skin from F1 MG-*albino* fish was dissected and GFP+ and GFP- cells were
166 isolated using FACS (Figure 2H). GFP+ cells encompass *mitfa*-expressing
167 melanocytes, xanthophores, and their progenitors, while GFP- cells represent other
168 non-melanocytic, non-*mitfa* expressing skin cells, such as keratinocytes, fibroblasts, and
169 immune cells. We performed CRISPR-seq on DNA from both populations to directly
170 measure Cas9 efficiency and cell-type specificity, quantifying the proportion of indels at
171 the *albino* locus. Although we have previously shown that FACS sorting melanocytic
172 cells is possible, it is important to note that we often observe high levels of
173 contaminating keratinocytes in FACS sorted melanocyte populations, which may lead to
174 an underestimation of the true allelic frequency in our CRISPR-seq[32]. Despite this,
175 robust inactivation of the *albino* gene was observed in GFP+ (*mitfa*-expressing) cells,
176 confirming somatic inactivation (Figure 2I). The majority of indels were frame-shift
177 inducing mutations. A likely PCR or sequencing artifact resulting in a “T” insertion was
178 excluded from the frameshift indel percentage as it was observed in all conditions
179 including WT fish with no pigmentation phenotype (Figure S2E). These results confirm
180 that our *mitfa*^{Cas9} system allows us to inactivate genes within the melanocytic lineage *in*
181 *vivo* in a cell-type specific manner.
182
183 **<u>The neural crest-related gene *sox10* has specific function in adult melanocyte</u>**
184 **<u>patterning and regeneration</u>**

185 Having confirmed that our *mitfa*^{Cas9} system allows us to manipulate melanocyte gene
186 expression, we next wanted to target embryonic essential genes. Detecting "negative"
187 gene knockout phenotypes such as cell death can be challenging *in vivo* due to the
188 selective advantage that WT cells have over mutants.
189
190 To assess the effectiveness of our *mitfa*^{Cas9} model in detecting negative phenotypes, we
191 utilized it to target *sox10*, a transcription factor vital to the neural crest lineage and
192 indispensable for overall survival of both zebrafish and mice[15,33]. Consequently, a global
193 knockout approach is not feasible for studying the function of *sox10* in adult
194 melanocytes *in vivo*. Germline knockout of *sox10* in zebrafish leads to severe defects in
195 peripheral nerve development and the complete absence of melanocytes, and the
196 animals die around day 14[15,34,35]. Due to the complete absence of melanocytes and
197 their precursor cells, melanoblasts, in *sox10*$^{-/-}$ fish, it has not been possible to study the
198 specific role of *sox10* on these more differentiated cell types *in vivo*. One of the key
199 unanswered questions is how *sox10* balances its role in maintaining melanoblast
200 stemness with promoting terminal differentiation, particularly in the context of adult
201 melanocyte regeneration.
202
203 We leveraged our *mitfa*^{Cas9} system to specifically inactivate *sox10* in the melanocyte
204 lineage. *mitfa*^{Cas9} fish injected with a MG-*sox10* plasmid exhibited noticeable gaps in
205 their melanocyte stripes (Figure 3A-B). Germline deletion of a *sox10* enhancer region
206 similarly affects adult stripe patterning in zebrafish[36]. In contrast to the *albino* F0 fish,
207 the gaps in the stripes of the *sox10* F0 fish were not occupied by unpigmented GFP+
208 melanocytes, indicating a potential defect in the survival or differentiation of
209 melanocytes upon loss of *sox10*. This phenotype became even more pronounced in the
210 stable F1 lines, where several gaps in the melanocyte stripes are visible (Figure 3C).
211 Zebrafish have four dark stripes occupied by melanocytes, which alternate with light
212 colored interstripes occupied by yellow pigmented xanthophores[37]. Typically,
213 melanocyte stripe 1D (dorsal) is wider than the interstripe X0 directly below it, as
214 observed in MG-NT F1 fish (Figure 3C-D). However, the opposite is true for MG-*sox10*
215 F1 fish, where we observed an apparent widening of the interstripe region and
216 narrowing of the melanocyte stripes (Figure 3C-D). Melanocytes were counted in fish
217 treated with epinephrine to aggregate melanosomes, revealing a significant reduction in
218 the number of melanocytes in the F1 *sox10* KO fish compared to F1 NT fish (Figure
219 3E). Reduction in GFP+ cells within the xanthophore interstripes (X0) suggested that
220 *sox10* deficiency also negatively affected xanthophore populations, in line with previous
221 work indicating a role for *sox10* in specifying both xanthophores and melanocytes in
222 zebrafish embryos[38].
223
224 Melanocytes continually regenerate throughout life, typically from a progenitor
225 population of melanoblasts or melanocyte stem cells. We next assessed whether *sox10*
226 was required for this. We treated adult fish with neocuproine, a copper chelator
227 previously shown to kill mature, pigmented melanocytes[39]. We then compared
228 regeneration from these progenitors in MG-*sox10* and MG-NT F1 fish by counting the
229 percentage of melanocytes that emerged after 7, 15, and 70 days (Figure 3F). At days 7
230 and 15, when the melanocytes were still in the process of regenerating from

melanoblasts, there were no significant differences between the two groups. However, by the time regeneration was completed we found a significant disparity between the regenerative potential of MG-NT and MG-*sox10* fish. At 70 days post-neocuproine treatment, MG-NT fish had regenerated an average of 82% of their melanocytes, whereas only 53% of melanocytes had regenerated in MG-*sox10* fish (Figures 3G-H). These findings demonstrate that *sox10* is required for adult melanocyte regeneration, highlighting its requirement within melanoblast populations outside of neural crest specification.

Non-autonomous functions of *tuba1a/tuba1c* on melanocytes

One of the significant challenges of conventional global knockout methods is the inability to differentiate between cell-autonomous and non-autonomous phenotypes. This distinction is particularly crucial in melanocyte studies due to their direct and indirect interactions with diverse cell types. A notable example of genes with pleiotropic effects is the tubulin gene family, whose α/β tubulin heterodimers form microtubules essential for various cellular processes such as cell division, motility, and intracellular transport across various cell types[40]. Microtubules are also critical for the transport of melanosomes in melanocytic cells[41].

Mutation of tubulin genes such as *tuba8l3a* in zebrafish leads to highly pleiotropic effects including defects in melanocyte patterning, CNS abnormalities, and altered craniofacial morphology[42]. We chose to focus on the closely related α tubulin gene *tuba1a*, which is highly expressed in many cell types of the developing zebrafish including melanocytes, but whose specific function in these cells remains unexplored[43]. Non-cell type specific knockout of *tuba1a* with the Alt-R CRISPR Cas9 system results in extensive embryo abnormalities including a curved tail phenotype, pericardial edema, and melanocytes with more dispersed pigmentation (Figure 4A-B, S3A-B). We found that compared to 71% survival of NT Alt-R embryos, only 10% of embryos injected with *tuba1a* Alt-R survive to 14dpf (Figure 4C). During validation of *tuba1a* Alt-R, we discovered that this guide also targets *tuba1c*, a gene with 99.78% homology to *tuba1a* in zebrafish (Figure S3B). Despite robust cutting, neither *tuba1a*- nor *tuba1c*-specific guides alone were sufficient to recreate the dispersed melanocyte phenotype (Figure S3C-D). However, we were able to recapitulate our findings using a second guide RNA that simultaneously targeted both *tuba1a* and *tuba1c*, suggesting possible redundancy of these genes, with compensation masking the phenotype in single-gene knockouts (Figure S4E-F).

Similar to *sox10,* the embryonic lethality of global *tuba1a/c* knockout prevents the study of knockout phenotypes in adult fish. To overcome this limitation, we implemented our *mitfa*^{Cas9} system to specifically knock out *tuba1a/c* in melanocytes (Figure S3G-H). CRISPR sequencing of GFP+ cells isolated from *mitfaCas9* MG-*tuba1a/c* fish confirmed successful knockout of both *tuba1a* and *tuba1c*, with knockout efficiencies comparable to those observed in MG-albino fish (Figure S3I). Unlike global knockout of *tuba1a/c*, melanocyte specific loss of *tuba1a/c* resulted in viable adult fish with no obvious abnormalities (Figure S3G-H). Surprisingly, we did not observe the dispersed melanocyte phenotype in any *mitfa*^{Cas9} MG-*tuba1a/c* embryos (Figure 4D-E). Based on

this observation, we hypothesized that *tuba1a/c* may be functioning in a cell non-autonomous manner on melanocytes.

The dispersed pigmentation observed in *tuba1a/c* Alt-R embryos resembles that seen in blind zebrafish, which fail to contract their melanosomes in response to light[44]. This light-mediated camouflage involves retinal ganglion cells signaling hypothalamic neurons to release melanin-concentrating hormone (MCH), which then binds to MCH receptors on melanocytes, triggering melanosome aggregation via microtubules[44]. The normal melanosome dispersion observed in *mitfa*^{Cas9} MG-*tuba1a/c* fish suggests that rather than a cell-intrinsic defect in melanosome aggregation, *tuba1a/c* may indirectly influence melanocytes through potential defects in retinal and/or central nervous system cells crucial for light-mediated camouflage. Interestingly, *TUBA1A* mutation in humans can result in both ophthalmologic and brain abnormalities and morpholino-based knockdown of *tuba1a* in zebrafish inhibits CNS development[45,46].

To further test this idea, we treated *tuba1a/c* Alt-R embryos with epinephrine to assess their ability to contract melanosomes in response to a non-visual stimulus. *Tuba1a/c* Alt-R embryos exposed to epinephrine had robust aggregation of melanosomes, demonstrating that the loss of *tuba1a/c* did not impair melanosome transport (Figure 4F-G). This finding further supports a non-autonomous role for *tuba1a/c* in melanocytes. Utilizing the *mitfa*^{Cas9} system distinguish cell-autonomous from non-autonomous gene functions provides valuable insights into the complex dynamics of cell-cell interactions and how genes function within cellular and organismal networks.

Targeting tumor suppressors with *mitfa*^{Cas9} induces melanoma

We next turned our attention to melanoma. In humans, tumor suppressors such as *PTEN* and *TP53* are somatically inactivated in melanoma[47,48]. In contrast, the most commonly used zebrafish models of melanoma use a germline *tp53* mutation, which is not typically seen in humans with the disease and precludes our ability to discern the role of *tp53* inactivation specifically in melanocytes and melanoma[49]. While global *tp53* loss is not lethal, it does lead to a wide range of non-melanoma tumors, which can deteriorate fish health and confound melanoma studies[50]. Furthermore, current zebrafish melanoma models typically involve the utilization of MiniCoopR *mitfa* rescue cassettes into *casper* or *nacre* zebrafish, which are devoid of normal pigment cells. Although this method is highly efficient, it does not accurately represent melanoma initiation in the context of normal skin architecture and relies on artificial overexpression of *mitfa*. To mimic human melanoma initiation more accurately, we used our *mitfa*^{Cas9} model to assess tumor initiation using melanoma-specific gene knockout in animals with wild-type skin. Previous studies have shown that expression of BRAF^{V600E} and loss of *tp53* in WT (non-*casper*) fish results in relatively low tumor burden, suggesting that the casper strain might be especially tumor prone in the setting of MiniCoopR *mitfa* rescue although the exact reasons for this are not clear. Based on this, to increase penetrance, we decided to also target *ptena* and *ptenb*, the zebrafish orthologs of human *PTEN*[51]. *Ptena/ptenb* loss in combination with *tp53* has been shown to accelerate melanoma formation in zebrafish[52,53].

To first address the effect of *ptena/b* loss on normal melanocytes, we generated melanocyte-specific knockouts of *ptena* and *ptenb* (Figure 5A). To visualize cells expressing both *ptena* and *ptenb* guides, we designed additional plasmids, denoted MTdT-gRNA, containing a zU6:gRNA cassette followed by *mitfa*:TdTomato and coinjected MG-*ptena* and MTdT-*ptenb* plasmids into *mitfa*^{Cas9} embryos. Like *sox10* and *tuba1a/c*, germline knockout of *ptena/b* is embryonic lethal[54,55]. In our *ptena/ptenb* F0 melanocyte-specific KO fish, survival was normal. We observed an aberrant expansion of the melanocytes outside of the stripe regions they normally are restrained to, suggesting that inactivation of *ptena* and *ptenb* induces defects in melanocyte patterning (Figure 5A and B). However, loss of *ptena/b* alone was not sufficient to induce melanoma.

To generate tumors, we co-injected *mitfa*^{Cas9} embryos with plasmids encoding *mitfa:*BRAF^{V600E} and sgRNAs targeting *tp53* and *ptena*/*b* (Figure 5C). Larvae were sorted for BFP+ eyes, indicating mitfa-Cas9 integration, and monitored for tumors over 30 weeks. No tumors were detected in BFP- fish from any of the injection conditions (n=136). We also did not observe any tumors in BFP+ fish injected with either BRAF^{V600E} alone (n=35) or ptena/b; *tp53* guides in the absence of BRAF^{V600E} (n=17). In contrast, tumors developed in all BFP+ groups injected with both *mitfa:*BRAF^{V600E} and gRNA plasmids. Approximately 5% of fish from the BRAF;*tp53* group developed tumors (Figure 5D). This aligns with a previous study where 6% of *tp53*-/- fish developed tumors when injected with a BRAF^{V600E} construct[51]. Targeting of *ptena* and *ptenb* in *mitfa*^{Cas9} fish co-injected with *mitfa*:BRAF^{V600E} resulted in a higher tumor incidence of 29% (Figure 5D).

When all three tumor suppressors (*tp53, ptena, ptenb*) were targeted in combination with BRAF^{V600E}, 59% of fish developed tumors by 30 weeks post fertilization (wpf) (Figure 5D). Immunohistochemistry (IHC) revealed that all tumor samples expressed BRAF^{V600E}, while p-AKT, a hallmark of *PTEN* inactivation, was only detected in samples with *ptena/b* KO (Figure 5E). To confirm on-target cutting, DNA was extracted from tumors and CRISPR sequencing was performed on PCR amplicons for each tumor suppressor gene. A large proportion of reads contained indels at the target locus for each of the target genes (*ptena*, *ptenb*, and *tp53*) (Figure 5F and S4A-C). Some tumors had an array of mutations, while others appeared to be composed largely of a one dominant clone (Figure S4A-C). Thus, similar to the MAZERATI system, our endogenous knockin system allows us to rapidly dissect the melanocyte-specific function of both oncogenes (BRAF^{V600E}), as well as putative tumor suppressors (*tp53*, *ptena/b*), while avoiding pleiotropic effects of global tumor suppressor loss.

<u>Targeting of lineage-specific oncogenes decreases tumor initiation but promotes progression</u>

Our next objective was to leverage the mitfa^{Cas9} fish as a tool for identifying or validating potential genetic dependencies within melanoma. Genetic dependencies can be difficult to study *in vivo* since inactivation of a required gene inevitably leads to selection for non-mutant alleles, as has been previously shown[56]. Large scale in vitro efforts such as the DepMap can provide guidance as to what genes are likely to be important for tumor

proliferation, but cell line studies alone cannot recapitulate the complex in vivo behavior that occurs from knocking individual genes out. In melanoma, the DepMap has identified *SOX10* as the top *in vitro* genetic dependency necessary for tumor cell proliferation, suggesting it acts as a lineage-specific oncogene[3,57]. In prior work in both zebrafish and mice, loss of *sox10* is clearly associated with a loss of tumor initiating potential and cell proliferation[56,57]. Yet its specific role *in vivo* remains unclear, since it is required for neural crest and melanocyte specification, making it difficult to know whether its effects reflect loss of the entire lineage[57]. Given our data above showing that *sox10* is required specifically in melanocyte patterning and regeneration, we wished to investigate its function in melanoma.

To assess this, we generated plasmids containing multiple sgRNAs driven by three distinct zU6 promoters (zU6A, zU6B, and zU6C) to simultaneously target both tumor suppressors (*tp53, ptena/ptenb*) and tumor promoting genes (*sox10*) in the same cells, which reduces the chance of selecting for non-mutant alleles[5]. We co-injected these plasmids with *mitfa*:BRAF^{V600E}, sorted fish for BFP+ eyes, and tracked tumor free survival over the course of 50 weeks (Figure 6A-B). Consistent with the DepMap prediction, *sox10* inactivation markedly reduced tumor incidence, which likely reflects loss of proliferation. Only 3/96 (3.1%) fish with *sox10* knockouts initiated melanomas compared to the 24/94 fish (25.5%) from the NT condition that developed tumors (Figure 6B). Using IHC, we validated that *sox10* KO tumors expressed lower levels of Sox10 protein compared to NT tumors (Figure 6C and S5A). Quantification of Sox10 intensity with immunofluorescence confirmed this finding (Figure S5B).

Although *sox10* clearly reduced tumor initiation, we noted “escapers”. These tumors appeared morphologically somewhat distinct compared to the *sox10* intact tumors. While not easily quantifiable, qualitatively based on prior experience, the tumor cells appeared more mesenchymal and penetrated more deeply under the skin than we typically see with the BRAF^{V600E} melanomas in the fish (Figure 6C). This observation raised the possibility that these tumors had undergone “phenotype switching”, a form of cell plasticity in which cells reversibly move between opposite extremes of proliferation versus invasive states[22,23,57,58]. In melanoma, the proliferative state is thought to be characterized by high expression of *SOX10*, whereas the mesenchymal, invasive state is characterized by high expression of *SOX9*[23]. These two highly related transcription factors have seemingly opposite and possibly antagonistic roles in melanoma. *In vitro*, knockout of *SOX10* in a variety of human cell lines is associated with acquisition of a *SOX9*^{hi} state, which has been suggested to be linked to the invasive phenotype[23]. We performed a re-analysis of publicly available RNA-seq data using 3 patient-derived human melanoma cell lines treated with siRNA targeting *SOX10* confirmed this observation, with the *SOX10* lines now becoming *SOX9*^{hi} (Figure 6E to J, S5C to L)[23]. These data raised the possibility that the more mesenchymal, invasive appearing tumors we see in our escaper fish might be due to gain of *sox9* expression. To test this, we stained our *sox10* CRISPR tumors for *sox9* and discovered that 2 of the 3 *sox10* KO tumors markedly upregulated *sox9* relative to control tumors expressing NT gRNA (Figure 6C and D). While this data is certainly not definitive, when taken in context of the above *in vitro* and *in vivo* data in other model systems, it appears consistent with the

idea that loss of *sox10* could result in more invasive tumors. This preliminary observation we have made will need further mechanistic dissection, and our system would be amenable to studying this phenomenon in further depth. This data also highlights that *in vitro* genetic studies such as the DepMap, which rely on proliferation as the readout, can mask more complex *in vivo* phenotypes.

Discussion:

The ability to model genetic dependencies *in vivo* is one of the most important uses of model organisms. Forward genetic mutagenesis screens using compounds such as ENU or EMS led to the identification of many key developmental genes in organisms such as Drosophila, C. elegans, Saccharomyces, zebrafish, and many others[59,60]. These approaches have rapidly accelerated in the era of TALENs and CRISPR, readily allowing for knockout of nearly any gene in a wide variety of non-model organisms. Cre/Lox approaches have further augmented our ability to discern the cell-type specific effects of these genes, although these are still laborious and time consuming, especially in models such as mice[13].

Alongside these approaches have been remarkable advances in large scale sequencing of human tissues. GWAS-like efforts such as the UK Biobank and the US All of Us programs have identified thousands of germline variants (SNPs) that may be linked to interesting phenotype variation[1,2]. A conceptually similar approach is also happening in diseases such as cancer, in which efforts such as the TCGA, ICGC and DepMap have continued to unveil new potential somatic variants (SNVs) linked to cancer[3,61,62].

Across these efforts, in both development and disease, the large number of candidate variants makes it challenging to connect these genotypes to phenotypes. This is especially acute in melanoma, where the large number of somatic variants generated by UV radiation leads to a high number of background mutations that may or may not have pathogenic function. Thus, there is a substantial need for *in vivo* models that allow for rapid and efficient modeling of candidate genes.

Prior work in the zebrafish has shown that promoter fragments driving Cas9 can provide efficient and scalable approaches to this problem[6,14]. For example, MAZERATI has been nicely applied to melanoma models to studying genetic dependencies in the melanocyte lineage[14]. The technology we describe in this work largely builds off the logic of this and related systems. One difference between our *mitfa*-Cas9 knockin line compared to MAZERATI is that it maintains the endogenous regulatory elements needed for control of the *mitfa* gene. We do not yet fully know when or if this difference would be important, but given the complex role of MITF transcription as a “rheostat” in melanoma[63], it is reasonable to assume these endogenous elements could become important in some circumstances. Because in our study we did not directly compare the *mitfa*-Cas9 knockin approach versus MAZERATI, we cannot make direct statements about which is more efficient. However, because both techniques reliably result in melanoma, each researcher will be able to choose the technology that is most appropriate for their biological question.

One advantage of Cas9 approaches in this system is the ability to screen phenotypes in both the F0 generation (as mosaics) or in the F1 generation (3 months later). Although the F0 phenotypes we observe are indeed subtle, they are still quantifiable. This enables rapid screening of candidate genes for melanocyte-specific functions. Promising hits can then be more specifically validated in the F1 generation, which is particularly advantageous for efficiently generating biallelic knockouts, especially for genes with recessive phenotypes like *albino*. On a per gene basis, this saves well over 3 months of work compared to germline recessive knockouts and eliminates the issue of inbreeding, promoting healthier genetic lines and facilitating the potential for outcrossing with any available fish line. Because we demonstrate that the Cas9 is completely restricted to the melanocyte lineage, with no detectable off-target expression, this easily allows us to discern the melanocyte-specific effect of pleiotropic genes very efficiently.

One interesting observation of our melanoma studies is evidence that loss of melanoma genetic dependencies like *SOX10* (as suggested by the human DepMap data) can still lead to a small number of tumors, albeit with seemingly different biological behaviors. In the human samples we analyzed, loss of *SOX10* leads to acquisition of a *SOX9*^{hi} state instead[23]. Similarly, in our "escaper" fish, we do see an increase in SOX9 expression in 2 out of 3 fish, which would be consistent with the human data. *SOX9* is increasingly recognized to be a potent mediator of tumor cell invasiveness, so it is possible this could explain the somewhat more mesenchymal/invasive appearance of these tumors[64,65]. This phenomenon clearly needs further study in future work, where the effect could be better quantified in a larger cohort and the relevant mechanism identified. But were this SOX10 to SOX9 switch hold up, one implication of this finding is that clinical targeting of transcription factors like *SOX10*[66], long considered an ideal therapeutic approach, could lead to unexpected outcomes in which tumors might proliferate less but become more invasive or resistant to therapy. Whether this phenomenon of *SOX10/SOX9* switching is a general phenomenon, or specific to that class of TFs, remains to be determined. However, a similar phenomenon has been observed for *MITF*, another melanocytic TF, suggesting this idea of TF switching needs to be more thoroughly explored in the future[58,67,68].

Finally, while our studies clearly focused on the melanocyte lineage, highly similar approaches could be taken for virtually any cellular lineage in which master regulators or markers are known. Given the large number of already identified promoter/enhancer fragments in the zebrafish, this would be an important extension of our system to study gene variants in the context of development and other diseases[69].

Our approach has several limitations that may need to be addressed in future studies. Due to the constitutive nature of the Cas9, we have little control over the timing of its expression. Because it is knocked into the endogenous *mitfa* locus, the expression of Cas9 will vary with the endogenous regulation of that gene. This may lead to somewhat paradoxical and unexpected results. For example, germline deletion of *sox10* results in the colourless phenotype, which is an animal completely devoid of melanocytes[15]. In contrast, when we knock out *sox10* specifically in the mitfa+ cells with our *mitfa*^{Cas9} system, we see a much more subtle phenotype, and not all melanocytes are lost. We

speculate this could be due to timing: the germline allele will already have loss of sox10 function very early in the development of the melanocyte lineage (i.e. at the neural crest stage), whereas our knockin approach will inactivate sox10 much later in development after melanocyte specification has already occurred. This could reflect different downstream targets of *sox10* in these two scenarios. In future iterations of this general approach, swapping the Cas9 for an inducible version would allow for better timed knockout of genes[70]. Because *mitfa* itself is expressed in melanoblasts, melanophores and xanthophores during different stages of development, choosing a promoter (e.g. PMEL) that is more tightly restricted to melanocytes may be advantageous. Another limitation is that our fish will result in a single functional copy of *mitfa*. While this does not result in any obvious phenotype (i.e. the melanocytes are normal) and this gene is not currently known to exhibit haploinsufficiency, it is possible that under certain circumstances the loss of one copy of *mitfa* could have unintended phenotypes. For example, in the tumor setting, having only one copy of *mitfa* could theoretically reduce tumor incidence since it can act as an oncogene in some situations[71]. This possibility of haploinsufficiency will need to be further explored in the future. Finally, although our system was relatively efficient, we still did not see 100% knockout. This may reflect that it is relatively easy to bypass the CRISPR lesion in an exon with an in-frame mutation. The use of multiple sgRNAs, or sgRNAs that target promoter regions, rather than exons, could further augment efficiency of knockout. Alternatively, instead of targeting DNA, we could consider using RNA targeting CRISPR enzymes. Recent work has shown that RNA degradation induced by Cas13 works in zebrafish and may allow for more nuanced knockdown rather than knockout of a given candidate gene[72,73]. This may especially have advantages in the context of melanoma, where genes are commonly dysregulated rather than completely knocked out. We envision it would be relatively straightforward to knock Cas13 into the locus of interest using an analogous approach to the one we have taken here.

Acknowledgements:
We thank members of the White lab for valuable discussions and feedback on this project. We also thank the MSKCC flow cytometry core for assistance with cell sorting, Integrated Genomics Operation Core, funded by an NCI Cancer Center Support Grant (P30 CA08748) for sequencing assistance, and Molecular Cytology Core for their help with imaging. We thank the MSKCC aquatics core facility for their support of this work. Schematic figures were all made using Biorender.com with a paid Biorender license.

Funding:
RMW was funded through the NIH/NCI Cancer Center Support Grant P30 CA008748, the Melanoma Research Alliance, The Debra and Leon Black Family Foundation, NIH Research Program Grants R01CA229215 and R01CA238317, NIH Director's New Innovator Award DP2CA186572, The Pershing Square Sohn Foundation, The Mark Foundation for Cancer Research, The American Cancer Society, The Alan and Sandra Gerry Metastasis Research Initiative at the Memorial Sloan Kettering Cancer Center, The Harry J. Lloyd Foundation, Consano and the Starr Cancer Consortium. This work was also supported by NIH ORIP R24OD020166 (MM). YM was supported by a Medical Scientist Training Program grant from the NIH under award number T32GM007739 to

the Weill Cornell/Rockefeller/Sloan Kettering Tri-Institutional MD-PhD Program and Kirschstein-National Research Service Award (NRSA) predoctoral fellowship under award number F30CA265124. MVH was funded by a K99/R00 Pathway to Independence Award from the National Cancer Institute (1K99CA266931). SP was funded by a Molecular Imaging in Cancer Biology Training Grant at Memorial Sloan Kettering Cancer Center from the National Cancer institute (T32CA254875) and the Ruth L. Kirschstein National Research Service Award for Individual Predoctoral Fellows from the National Cancer Institute (F31CA271518).

Author Contributions:

Conceptualization: SP, RMW
Investigation: SP, YM, MVH, JBS, NMC, ZM, JX
Visualization: SP, MVH, JBS
Supervision: TL, MM, RMW
Writing—original draft: SP, RMW
Writing—review & editing: SP, MVH, NMC, RMW

Declaration of Interests:

MM has competing interests with Recombinetics Inc., LifEngine Technologies, and LifEngine Animal Health Laboratories, Inc. RMW is a paid consultant to N-of-One Therapeutics, a subsidiary of Qiagen and is on the scientific advisory board of Consano but receives no income for this. RMW receives royalty payments for the use of the *casper* zebrafish line from Carolina Biologicals. SP, YM, MVH, JBS, NMC, ZM, JX, and TL declare no competing interests.

Methods

Materials Availability: All data are available in the main text or the supplementary materials, or upon request. Plasmids, fish lines and other materials generated from this study are available upon request.

Zebrafish husbandry and ethics statement

All zebrafish experiments adhered to institutional animal protocols and were conducted in compliance with approved procedures. Fish stocks were maintained at a temperature of 28.5 °C, under 14:10 light:dark cycles, with pH set at 7.4, and salinity-controlled conditions. The zebrafish were fed a standard diet comprising brine shrimp followed by Zeigler pellets. Approval for the animal protocols outlined in this manuscript was obtained from the Memorial Sloan Kettering Cancer Center (MSKCC) Institutional Animal Care and Use Committee (IACUC), under protocol number 12-05-008. Anesthesia was conducted using Tricaine (4 g/l, Syndel, Ferndale, WA, USA) from a stock of 4 g/l and diluted to 0.16 mg/ml. Adult zebrafish of both sexes were equally employed in all experiments. Embryos, collected through natural mating, were incubated in E3 buffer (5 mM NaCl, 0.17 mM KCl, 0.33 mM CaCl2, 0.33 mM MgSO4) at 28.5 °C. The wild-type strain used was Tropical 5D Zebrafish (T5D)[27].

599 **GeneWeld plasmid construction**
600 A combination of restriction enzyme digestion and HiFi cloning was used to construct
601 the GeneWeld pPRISM-nCas9n, γcry1:BFP vector for targeted integration to isolate an
602 nls-Cas9-nls knockin. A 765 bp fragment containing the Porcine teschovirus-1
603 polyprotein 2A peptide sequence was amplified from the pPRISM-2A-Cre, γcry1:BFP
604 vector (Addgene #117789) with primers Ori-F and 2A-R[24,25]. The nCas9n cDNA was
605 amplified from the expression vector pT3TS-nCas9n (Addgene #46757) with primers
606 Cas9-F and Cas9-R[74]. A KpnI/SpeI fragment containing the pPRISM-2A-Cre, gcry1:BFP
607 vector backbone was assembled with the 2A and nCas9n PCR amplicons using the
608 NEBuilder HiFi DNA Assembly Cloning Kit (NEB # E5520S) following the
609 manufacturer's instructions.
610
611 Homology arms were designed as previously described[24,25]. Briefly, 48bp homology
612 arms complementary to the *mitfa* target site were designed using GTagHD
613 (http://www.genesculpt.org/gtaghd/) for the pPRISM GeneWeld plasmid series. The two
614 pairs of complementary oligos can be found in Table S1. 5' and 3' arms were cloned
615 sequentially into the pPRISM-nCas9n, γcry1:BFP vector. The 3' homology arm oligos
616 were annealed and cloned into the vector using the BspQI restriction site as previously
617 described. Due to the multiple BfuAI sites within Cas9, instead of using BfuAI restriction
618 cloning, we alternatively used in-fusion cloning (Takara Bio) to insert a gBlock (IDT)
619 containing the 5' homology arm into the pPRISM-nCas9n, gcry1:BFP vector. Primers
620 and gblock sequence used for cloning are listed in Table S1. The 5' and 3' homology
621 arms were sequenced with primers 5'homologycheckF and R3'_pgtag_seq,
622 respectively.
623
624 **Injection of GeneWeld reagents**
625 Injections of GeneWeld reagents were performed on one-cell stage embryos. We used
626 the Alt-R CRISPR-Cas9 system (IDT) for the initial knock-in of nCas9n, γcry1:BFP to
627 the *mitfa* locus. In brief, 100 μM tracrRNA (IDT 1075928) was mixed at a 1:1 ratio with
628 either *mitfa* crRNA or universal crRNA then incubated at 95 °C for 5 min. Recombinant
629 Cas9 (IDT 1081059) was incubated with both sgRNAs for 10 min at 37 °C to form the
630 RNP complex. The GeneWeld pPRISM-5'mitfaHom-nCas9n, gcry1:BFP-3'mitfaHom
631 plasmid was then added to the injection mix along with phenol red (Sigma-Aldrich
632 P0290). The final concentrations injected into the embryos were: 75 pg/nl Cas9, 12.5
633 pg/nl *mitfa* sgRNA, 12.5 pg/nl Universal sgRNA, and 5 pg/nl pPRISM plasmid.
634
635 **Genotyping**
636 Tail clips were taken from 2 month postfertilization (mpf) zebrafish and DNA was
637 extracted using the DNeasy Blood and tissue kit (Qiagen). DNA was PCR amplified with
638 Q5 high fidelity DNA polymerase (NEB). The forward primer MitfaPCR-F binds to the
639 *mitfa* genomic region upstream of the insertion site and the reverse primer
640 5'homology_amplify-R binds the p2A region of the insertion cassette. Expected PCR
641 amplicon size is 269bp. Amplicons were sequenced using sanger sequencing (Azenta
642 Life Sciences).
643
644 **RNA-FISH HCR**

645 We adapted the HCR protocol from Ibarra-Garcia-Padilla et al.[75]. Briefly, embryos were
646 collected and treated with 0.0045% 1-phenyl 2-thiourea (PTU) (Sigma-Aldrich) after 24
647 hpf to block pigmentation. Embryos were harvested at 72 hpf and fixed in 4% PFA
648 (Santa Cruz) for 24 hrs at 4 °C. Embryos were then washed with PBS and
649 dehydrated/permeabilized with a series of MeOH (Millipore) washes. Embryos were
650 rehydrated with a series of MeOH/PBST washes, permeabilized with acetone (Fisher
651 Scientific) and incubated with Proteinase K (Millipore) for 30 min. This was followed by
652 further fixation with 4% PFA. Embryos were pre-hybridized in probe hybridization buffer
653 (PHB) before incubating them with HCR probes in PHB at concentration of 20nM. Probe
654 sequences for *mitfa* and Cas9 can be found in Table S1. Embryos were washed with
655 probe wash buffer before being pre-amplified with probe amplification buffer (PAB).
656 Following pre-amplification, amplifier hairpins were thawed, snap-cooled, and mixed
657 with PAB to a concentration of 36 nM. Embryos were incubated in the hairpin solution
658 followed by washes with 5×SSCT and 1× PBST. Embryos were stained with 2 µg/mL
659 DAPI in PBST and mounted on glass slides. Imaging was performed using a Zeiss
660 LSM880 confocal microscope. Melanocytes were assessed for co-expression of *mitfa*
661 and Cas9 within a 212-micron long section of the embryo, located directly caudal to the
662 yolk and typically encompassing 3–5 distinct midline melanocytes per embryo. Overlap
663 in expression was assessed using Fiji.
664
665 **Guide RNA plasmids**
666 The following plasmids were constructed using the Gateway Tol2kit:
667 zU6A:gRNA-NT;zU6B:gRNA-*ptena*;zU6C:gRNA-*tp53*/394,
668 zU6A:gRNA-NT;zU6B:gRNA-*ptenb*;zU6C:gRNA-*tp53*/394,
669 zU6A:gRNA-*sox10*;zU6B:gRNA-*ptena*;zU6C:gRNA-*tp53*/394,
670 zU6A:gRNA-*sox10*;zU6B:gRNA-*ptenb*;zU6C:gRNA-*tp53*/394.
671
672 In-fusion cloning (Takara Bio) was used to insert *mitfa:*GFP or *mitfa:*TdTomato into a
673 zU6:gRNA/394 plasmid previously developed in the lab (See Table S1 for primers
674 used). gRNAs were cloned into zU6:gRNA;*mitfa:*GFP/394 or
675 zU6:gRNA;*mitfa:*TdTomato/394 using BsmBI sites. Other plasmids used in this study
676 that were previously developed in the lab include zU6:gRNA-*ptena*/394, zU6:gRNA-
677 *ptenb*/394, zU6:gRNA-*tp53*/394, *mitfa*-BRAF^{V600E};cmlc2:eGFP. All guide RNAs used in
678 this study besides *tuba1a/c* have previously been validated in zebrafish[24,32,56,76].
679
680 **Validation of *tuba1a/c* sgRNAs**
681 The Alt-R CRISPR-Cas9 system (IDT) was used to achieve non-cell type specific
682 knockout of *tuba1a/c.* Guide RNAs were designed using ChopChop[77]. In brief, 100 µM
683 tracrRNA (IDT 1075928) was mixed at a 1:1 ratio with crRNA then incubated at 95 °C
684 for 5 min. Recombinant Cas9 (IDT 1081059) was incubated with the sgRNA for 10 min
685 at 37 °C to form the RNP complex. Phenol red was added prior to injection into 1 cell-
686 stage wild-type T5D embryos. To validate on-target cutting, 4 embryos were pooled and
687 DNA was extracted using Quick Extract buffer (Fisher Scientific NC0302740). DNA was
688 PCR amplified with Q5 high fidelity DNA polymerase (NEB) and forward and reverse
689 primers (Table S1). Exosap IT for PCR Product Clean Up was added to PCR product

690 prior to sanger sequencing. Forward and reverse primers used for PCR amplification
691 were also used for sequencing (Table S1).
692
693 **Transgenic lines**
694 To generate MG-U6:sgRNA stable lines, one-cell-stage embryos from crossing WT and
695 mitfa:Cas9 fish were collected and injected with the 30 pg indicated plasmid and 20 pg
696 tol2 mRNA. Fish with GFP+ melanocytes and BFP+ eyes were selected and outcrossed
697 with WT fish to produce the F1 generation. F1 fish were again sorted and outcrossed to
698 generate F2 generation zebrafish. All fish were imaged on a Zeiss AxioZoom V16 with
699 Zen 2.1 software.
700
701 **Flow cytometry of melanocytes from adult zebrafish**
702 Zebrafish were euthanized using ice-cold water and dissected using a clean scalpel and
703 forceps. The epidermal and dermal layers of the skin as well as the fins were separated
704 from the rest of the tissues and diced into 1-3mm pieces. Cells were dissociated with
705 Liberase TL (Millipore Sigma 05401020001) and filtered for single cell suspensions as
706 previously described[32]. Samples were then FACS sorted (BD FACSAria) for GFP+ and
707 GFP- cells. WT fish were used as a GFP negative control. Genomic DNA was isolated
708 from sorted cells using the DNeasy Blood and Tissue Kit (Qiagen).
709
710 **Tumor Dissection**
711 Fish with tumors were euthanized with ice-cold water and immediately dissected with a
712 scalpel to isolate tumor tissue. Genomic DNA was purified from the tumor samples
713 using the Dneasy Blood and tissue kit (Qiagen).
714
715 **CRISPR sequencing**
716 Primer pairs were designed to produce amplicons 200 to 280 bp in length with the
717 mutation site within 100 bp from the beginning or end of amplicon (see Table S1 for
718 primer sequences). Genomic DNA isolated from methods detailed above was PCR
719 amplified with Q5 high fidelity DNA polymerase (NEB) and run on an agarose gel to
720 visualize PCR products. The samples were then purified using the NucleoSpin Gel and
721 PCR cleanup kit (Takara Bio). Deep sequencing was conducted using the CRISPR-seq
722 platform. Sequencing data was analyzed with CRISPResso2[78]. and indel charts were
723 generated with CRISPRVariants R package[79].
724
725 **Drug treatments**
726 Adult zebrafish were treated for 24 hr with 750nM neocuproine (Sigma-Aldrich)
727 dissolved in fish water with a final concentration of 0.0075% DMSO as previously
728 described[39]. Cells from the middle melanocyte stripe were counted within a rectangular
729 region of 4mm x 1.5mm. Epinephrine hydrochloride (Sigma-Aldrich) was used at 1
730 mg/ml in fish water. Fish were treated for 10 minutes prior to imaging.
731
732 **Zebrafish tumor-free survival curves**
733 To generate a transgenic melanoma model, one-cell-stage embryos from WT X
734 mitfa:Cas9 fish crosses were injected with *mitfa*-BRAF^{V600E};cmlc2:eGFP, 20 pg Tol2
735 mRNA, and the indicated gRNA plasmids for each condition. The total amount of

736 plasmid per embryo did not exceed 30 pg. Embryos were screened for GFP positive
737 hearts and sorted for BFP+ or BFP- eyes. Fish were screened for tumors using a
738 microscope every 2 weeks starting at 4 weeks post fertilization. Tumors were only
739 called if an elevated lesion was observed. Graphpad prism 9 was used to generate and
740 analyze Kaplan-Meier survival curves. Statistical differences were determined using log-
741 rank Mantel–Cox test. All screening and imaging was conducted on a Zeiss AxioZoom
742 V16 using Zen 2.1 software.
743
744 **Histology**
745 Zebrafish were sacrificed using ice-cold water and placed in 4% paraformaldehyde
746 (Santa Cruz 30525-89-4) in PBS for 72 h at 4°C on a rocker. Fish were then transferred
747 to 70% EtOH for 24 h at 4°C on a rocker. Fish were sent to Histowiz, Inc (Brooklyn, NY,
748 USA), where they were paraffin embedded, sectioned, stained and imaged. All the
749 stainings were performed at Histowiz, Inc Brooklyn, using the Leica Bond RX automated
750 stainer (Leica Microsystems) using a Standard Operating Procedure and fully
751 automated workflow. Samples were processed, embedded in paraffin, and sectioned at
752 4µm. The slides were dewaxed using xylene and alcohol based dewaxing solutions.
753 Epitope retrieval was performed by heat-induced epitope retrieval (HIER) of the
754 formalin-fixed, paraffin-embedded tissue using Citrate based pH 6 solution (Leica
755 Microsystems, AR9961) for 20 mins at 95 C. The tissues were first incubated with
756 peroxide block buffer (Leica Microsystems), followed by incubation with the following
757 antibodies for 30 min: BRAFV600E antibody (ab228461, 1:100), phospho-AKT antibody
758 (CST4060, 1:50), SOX9 antibody (AB_185230, 1:1000), and SOX10 antibody
759 (GTX128374, 1:500). This was followed by incubation with DAB secondary reagents:
760 polymer, DAB refine and hematoxylin (Bond Polymer Refine Detection Kit, Leica
761 Microsystems) according to the manufacturer's protocol. The slides were dried,
762 coverslipped (TissueTek-Prisma Coverslipper) and visualized using a Leica Aperio AT2
763 slide scanner (Leica Microsystems) at 40X.
764
765
766 **Quantification of Sox10 intensity**
767 FFPE slides were deparaffinized by consecutive incubations in xylene and 100-50%
768 ethanol. For antigen retrieval, slides were placed in 10 mM sodium citrate pH 6.2 in a
769 pressure cooker and heated to 95°C for 20 minutes. Slides were then cooled to room
770 temperature and blocked in 5% donkey serum, 1% BSA, and 0.4% Triton-X100 in PBS
771 for 1 hour at room temperature. The primary antibody targeting Sox10 (GeneTex,
772 GTX128374) was added to the blocking buffer at 1:200 concentration and incubated at
773 4°C overnight. Slides were then washed in PBS before incubation with the secondary
774 antibody (donkey anti-rabbit Alexa Fluor Plus 488, Thermo Fisher Scientific #AC32790;
775 1:250) and Hoescht (Thermo Fisher Scientific, #62249; 1:1000) in blocking buffer for 2
776 hours at room temperature. Slides were mounted in Vectashield Plus (Vector Labs, H-
777 1900). Slides were imaged on a LSM 880 confocal microscope using a 40X oil
778 immersion objective. 3 images were captured per sample. Quantification of Sox10
779 intensity per cell was performed using CellProfiler[80] and MATLAB r2023b (Mathworks).
780 Cells were segmented in CellProfiler to obtain a nuclear mask from the Hoescht signal
781 and using this mask the mean intensity per nucleus was quantified.

782
783 **Re-analysis of human melanoma scRNA-seq data**
784 Human melanoma scRNA-seq data from Wouters et al. was accessed from GEO
785 (GSE134432)[23]. All analysis was done in R (version 4.3.1) using the Seurat package
786 (version 5.0.2)[81]. Counts matrices for each sample and cell line were imported into R
787 using the function read.table and converted into Seurat objects with the function
788 CreateSeuratObject before merging into one combined Seurat object using the function
789 merge. Counts were normalized using the Seurat function NormalizeData with default
790 parameters. UMAP was calculated using the Seurat function RunUMAP with 10
791 dimensions. SOX10 expression was plotted using the functions FeaturePlot and
792 VlnPlot.
793
794
795 **Statistical analysis**
796 Statistical significance was analyzed using t test, Log-rank (Mantel-Cox) test, Wilcoxon
797 Rank Sum Test or as indicated in the figure legends. GraphPad Prism 9 software was
798 used for data processing and statistical analysis. *P < 0.05; **P < 0.005; ***P < 0.001;
799 ****P < 0.0001. Data are presented as means ± SD unless otherwise indicated.
800
801 **References**

802 1 Mayer, C. S. & Huser, V. Learning important common data elements from shared
803 study data: The All of Us program analysis. *PLoS One* **18**, e0283601 (2023).
804 https://doi.org/10.1371/journal.pone.0283601
805 2 Sudlow, C. *et al.* UK biobank: an open access resource for identifying the causes
806 of a wide range of complex diseases of middle and old age. *PLoS Med* **12**,
807 e1001779 (2015). https://doi.org/10.1371/journal.pmed.1001779
808 3 Tsherniak, A. *et al.* Defining a Cancer Dependency Map. *Cell* **170**, 564-576 e516
809 (2017). https://doi.org/10.1016/j.cell.2017.06.010
810 4 Amsterdam, A. *et al.* Identification of 315 genes essential for early zebrafish
811 development. *Proc Natl Acad Sci U S A* **101**, 12792-12797 (2004).
812 https://doi.org/10.1073/pnas.0403929101
813 5 Yin, L. *et al.* Multiplex Conditional Mutagenesis Using Transgenic Expression of
814 Cas9 and sgRNAs. *Genetics* **200**, 431-441 (2015).
815 https://doi.org/10.1534/genetics.115.176917
816 6 Ablain, J., Durand, E. M., Yang, S., Zhou, Y. & Zon, L. I. A CRISPR/Cas9 vector
817 system for tissue-specific gene disruption in zebrafish. *Dev Cell* **32**, 756-764
818 (2015). https://doi.org/10.1016/j.devcel.2015.01.032
819 7 Zhou, W. *et al.* Neutrophil-specific knockout demonstrates a role for mitochondria
820 in regulating neutrophil motility in zebrafish. *Dis Model Mech* **11** (2018).
821 https://doi.org/10.1242/dmm.033027
822 8 Ni, T. T. *et al.* Conditional control of gene function by an invertible gene trap in
823 zebrafish. *Proc Natl Acad Sci U S A* **109**, 15389-15394 (2012).
824 https://doi.org/10.1073/pnas.1206131109
825 9 Grajevskaja, V., Camerota, D., Bellipanni, G., Balciuniene, J. & Balciunas, D.
826 Analysis of a conditional gene trap reveals that tbx5a is required for heart

827 regeneration in zebrafish. *PLoS One* **13**, e0197293 (2018).
828 https://doi.org/10.1371/journal.pone.0197293
829 10 Burg, L. *et al.* Conditional mutagenesis by oligonucleotide-mediated integration of
830 loxP sites in zebrafish. *PLoS Genet* **14**, e1007754 (2018).
831 https://doi.org/10.1371/journal.pgen.1007754
832 11 Kalvaityte, M. & Balciunas, D. Conditional mutagenesis strategies in zebrafish.
833 *Trends Genet* **38**, 856-868 (2022). https://doi.org/10.1016/j.tig.2022.04.007
834 12 Singh Angom, R., Wang, Y., Wang, E., Dutta, S. K. & Mukhopadhyay, D.
835 Conditional, Tissue-Specific CRISPR/Cas9 Vector System in Zebrafish Reveals
836 the Role of Nrp1b in Heart Regeneration. *Arterioscler Thromb Vasc Biol* **43**,
837 1921-1934 (2023). https://doi.org/10.1161/ATVBAHA.123.319189
838 13 Shin, M. *et al.* Generation and application of endogenously floxed alleles for cell-
839 specific knockout in zebrafish. *Dev Cell* **58**, 2614-2626 e2617 (2023).
840 https://doi.org/10.1016/j.devcel.2023.07.022
841 14 Ablain, J., Liu, S., Moriceau, G., Lo, R. S. & Zon, L. I. SPRED1 deletion confers
842 resistance to MAPK inhibition in melanoma. *J Exp Med* **218** (2021).
843 https://doi.org/10.1084/jem.20201097
844 15 Dutton, K. A. *et al.* Zebrafish colourless encodes sox10 and specifies non-
845 ectomesenchymal neural crest fates. *Development* **128**, 4113-4125 (2001).
846 https://doi.org/10.1242/dev.128.21.4113
847 16 Parichy, D. M. *et al.* Mutational analysis of endothelin receptor b1 (rose) during
848 neural crest and pigment pattern development in the zebrafish Danio rerio. *Dev*
849 *Biol* **227**, 294-306 (2000). https://doi.org/10.1006/dbio.2000.9899
850 17 Eom, D. S., Patterson, L. B., Bostic, R. R. & Parichy, D. M. Immunoglobulin
851 superfamily receptor Junctional adhesion molecule 3 (Jam3) requirement for
852 melanophore survival and patterning during formation of zebrafish stripes. *Dev*
853 *Biol* **476**, 314-327 (2021). https://doi.org/10.1016/j.ydbio.2021.04.007
854 18 Parichy, D. M. & Turner, J. M. Zebrafish puma mutant decouples pigment pattern
855 and somatic metamorphosis. *Dev Biol* **256**, 242-257 (2003).
856 https://doi.org/10.1016/s0012-1606(03)00015-0
857 19 Nguyen, P. D. *et al.* Haematopoietic stem cell induction by somite-derived
858 endothelial cells controlled by meox1. *Nature* **512**, 314-318 (2014).
859 https://doi.org/10.1038/nature13678
860 20 Irion, U., Singh, A. P. & Nusslein-Volhard, C. The Developmental Genetics of
861 Vertebrate Color Pattern Formation: Lessons from Zebrafish. *Curr Top Dev Biol*
862 **117**, 141-169 (2016). https://doi.org/10.1016/bs.ctdb.2015.12.012
863 21 Parichy, D. M., Rawls, J. F., Pratt, S. J., Whitfield, T. T. & Johnson, S. L.
864 Zebrafish sparse corresponds to an orthologue of c-kit and is required for the
865 morphogenesis of a subpopulation of melanocytes, but is not essential for
866 hematopoiesis or primordial germ cell development. *Development* **126**, 3425-
867 3436 (1999). https://doi.org/10.1242/dev.126.15.3425
868 22 Capparelli, C. *et al.* Targeting SOX10-deficient cells to reduce the dormant-
869 invasive phenotype state in melanoma. *Nat Commun* **13**, 1381 (2022).
870 https://doi.org/10.1038/s41467-022-28801-y

23 Wouters, J. *et al.* Robust gene expression programs underlie recurrent cell states and phenotype switching in melanoma. *Nat Cell Biol* **22**, 986-998 (2020). https://doi.org/10.1038/s41556-020-0547-3

24 Welker, J. M. *et al.* GeneWeld: Efficient Targeted Integration Directed by Short Homology in Zebrafish. *Bio Protoc* **11**, e4100 (2021). https://doi.org/10.21769/BioProtoc.4100

25 Wierson, W. A. *et al.* Efficient targeted integration directed by short homology in zebrafish and mammalian cells. *Elife* **9** (2020). https://doi.org/10.7554/eLife.53968

26 White, R. M. *et al.* Transparent adult zebrafish as a tool for in vivo transplantation analysis. *Cell Stem Cell* **2**, 183-189 (2008). https://doi.org/10.1016/j.stem.2007.11.002

27 Balik-Meisner, M., Truong, L., Scholl, E. H., Tanguay, R. L. & Reif, D. M. Population genetic diversity in zebrafish lines. *Mamm Genome* **29**, 90-100 (2018). https://doi.org/10.1007/s00335-018-9735-x

28 Lister, J. A., Robertson, C. P., Lepage, T., Johnson, S. L. & Raible, D. W. nacre encodes a zebrafish microphthalmia-related protein that regulates neural-crest-derived pigment cell fate. *Development* **126**, 3757-3767 (1999). https://doi.org/10.1242/dev.126.17.3757

29 Fernandez, L. P. *et al.* SLC45A2: a novel malignant melanoma-associated gene. *Hum Mutat* **29**, 1161-1167 (2008). https://doi.org/10.1002/humu.20804

30 Branicki, W., Brudnik, U., Draus-Barini, J., Kupiec, T. & Wojas-Pelc, A. Association of the SLC45A2 gene with physiological human hair colour variation. *J Hum Genet* **53**, 966-971 (2008). https://doi.org/10.1007/s10038-008-0338-3

31 Streisinger, G., Singer, F., Walker, C., Knauber, D. & Dower, N. Segregation analyses and gene-centromere distances in zebrafish. *Genetics* **112**, 311-319 (1986). https://doi.org/10.1093/genetics/112.2.311

32 Weiss, J. M. *et al.* Anatomic position determines oncogenic specificity in melanoma. *Nature* **604**, 354-361 (2022). https://doi.org/10.1038/s41586-022-04584-6

33 Hou, L., Arnheiter, H. & Pavan, W. J. Interspecies difference in the regulation of melanocyte development by SOX10 and MITF. *Proc Natl Acad Sci U S A* **103**, 9081-9085 (2006). https://doi.org/10.1073/pnas.0603114103

34 Kelsh, R. N. *et al.* Zebrafish pigmentation mutations and the processes of neural crest development. *Development* **123**, 369-389 (1996). https://doi.org/10.1242/dev.123.1.369

35 Carney, T. J. *et al.* A direct role for Sox10 in specification of neural crest-derived sensory neurons. *Development* **133**, 4619-4630 (2006). https://doi.org/10.1242/dev.02668

36 Cunningham, R. L. *et al.* Functional in vivo characterization of sox10 enhancers in neural crest and melanoma development. *Commun Biol* **4**, 695 (2021). https://doi.org/10.1038/s42003-021-02211-0

37 Owen, J. P., Kelsh, R. N. & Yates, C. A. A quantitative modelling approach to zebrafish pigment pattern formation. *Elife* **9** (2020). https://doi.org/10.7554/eLife.52998

38 Nagao, Y. *et al.* Distinct interactions of Sox5 and Sox10 in fate specification of pigment cells in medaka and zebrafish. *PLoS Genet* **14**, e1007260 (2018). https://doi.org/10.1371/journal.pgen.1007260

39 O'Reilly-Pol, T. & Johnson, S. L. Neocuproine ablates melanocytes in adult zebrafish. *Zebrafish* **5**, 257-264 (2008). https://doi.org/10.1089/zeb.2008.0540

40 Cushion, T. D., Leca, I. & Keays, D. A. MAPping tubulin mutations. *Front Cell Dev Biol* **11**, 1136699 (2023). https://doi.org/10.3389/fcell.2023.1136699

41 Rogers, S. L., Tint, I. S., Fanapour, P. C. & Gelfand, V. I. Regulated bidirectional motility of melanophore pigment granules along microtubules in vitro. *Proc Natl Acad Sci U S A* **94**, 3720-3725 (1997). https://doi.org/10.1073/pnas.94.8.3720

42 Larson, T. A., Gordon, T. N., Lau, H. E. & Parichy, D. M. Defective adult oligodendrocyte and Schwann cell development, pigment pattern, and craniofacial morphology in puma mutant zebrafish having an alpha tubulin mutation. *Dev Biol* **346**, 296-309 (2010). https://doi.org/10.1016/j.ydbio.2010.07.035

43 Farnsworth, D. R., Saunders, L. M. & Miller, A. C. A single-cell transcriptome atlas for zebrafish development. *Dev Biol* **459**, 100-108 (2020). https://doi.org/10.1016/j.ydbio.2019.11.008

44 Neuhauss, S. C. *et al.* Genetic disorders of vision revealed by a behavioral screen of 400 essential loci in zebrafish. *J Neurosci* **19**, 8603-8615 (1999). https://doi.org/10.1523/JNEUROSCI.19-19-08603.1999

45 Myers, K. A., Bello-Espinosa, L. E., Kherani, A., Wei, X. C. & Innes, A. M. TUBA1A Mutation Associated With Eye Abnormalities in Addition to Brain Malformation. *Pediatr Neurol* **53**, 442-444 (2015). https://doi.org/10.1016/j.pediatrneurol.2015.07.004

46 Veldman, M. B., Bemben, M. A. & Goldman, D. Tuba1a gene expression is regulated by KLF6/7 and is necessary for CNS development and regeneration in zebrafish. *Mol Cell Neurosci* **43**, 370-383 (2010). https://doi.org/10.1016/j.mcn.2010.01.004

47 Roh, M. R. *et al.* Promoter Methylation of PTEN Is a Significant Prognostic Factor in Melanoma Survival. *J Invest Dermatol* **136**, 1002-1011 (2016). https://doi.org/10.1016/j.jid.2016.01.024

48 Palmieri, G. *et al.* Multiple Molecular Pathways in Melanomagenesis: Characterization of Therapeutic Targets. *Front Oncol* **5**, 183 (2015). https://doi.org/10.3389/fonc.2015.00183

49 Frantz, W. T. & Ceol, C. J. From Tank to Treatment: Modeling Melanoma in Zebrafish. *Cells* **9** (2020). https://doi.org/10.3390/cells9051289

50 Ignatius, M. S. *et al.* tp53 deficiency causes a wide tumor spectrum and increases embryonal rhabdomyosarcoma metastasis in zebrafish. *Elife* **7** (2018). https://doi.org/10.7554/eLife.37202

51 Patton, E. E. *et al.* BRAF mutations are sufficient to promote nevi formation and cooperate with p53 in the genesis of melanoma. *Curr Biol* **15**, 249-254 (2005). https://doi.org/10.1016/j.cub.2005.01.031

52 He, S. *et al.* Synergistic melanoma cell death mediated by inhibition of both MCL1 and BCL2 in high-risk tumors driven by NF1/PTEN loss. *Oncogene* **40**, 5718-5729 (2021). https://doi.org/10.1038/s41388-021-01926-y

53 Montal, E., Suresh, S., Ma, Y., Tagore, M. M. & White, R. M. Cancer Modeling by Transgene Electroporation in Adult Zebrafish (TEAZ). *Methods Mol Biol* **2707**, 83-97 (2024). https://doi.org/10.1007/978-1-0716-3401-1_5

54 Croushore, J. A. *et al.* Ptena and ptenb genes play distinct roles in zebrafish embryogenesis. *Dev Dyn* **234**, 911-921 (2005). https://doi.org/10.1002/dvdy.20576

55 Faucherre, A., Taylor, G. S., Overvoorde, J., Dixon, J. E. & Hertog, J. Zebrafish pten genes have overlapping and non-redundant functions in tumorigenesis and embryonic development. *Oncogene* **27**, 1079-1086 (2008). https://doi.org/10.1038/sj.onc.1210730

56 Kaufman, C. K. *et al.* A zebrafish melanoma model reveals emergence of neural crest identity during melanoma initiation. *Science* **351**, aad2197 (2016). https://doi.org/10.1126/science.aad2197

57 Shakhova, O. *et al.* Antagonistic cross-regulation between Sox9 and Sox10 controls an anti-tumorigenic program in melanoma. *PLoS Genet* **11**, e1004877 (2015). https://doi.org/10.1371/journal.pgen.1004877

58 Hoek, K. S. *et al.* In vivo switching of human melanoma cells between proliferative and invasive states. *Cancer Res* **68**, 650-656 (2008). https://doi.org/10.1158/0008-5472.CAN-07-2491

59 Solnica-Krezel, L., Schier, A. F. & Driever, W. Efficient recovery of ENU-induced mutations from the zebrafish germline. *Genetics* **136**, 1401-1420 (1994). https://doi.org/10.1093/genetics/136.4.1401

60 Russell, W. L. *et al.* Specific-locus test shows ethylnitrosourea to be the most potent mutagen in the mouse. *Proc Natl Acad Sci U S A* **76**, 5818-5819 (1979). https://doi.org/10.1073/pnas.76.11.5818

61 Cerami, E. *et al.* The cBio cancer genomics portal: an open platform for exploring multidimensional cancer genomics data. *Cancer Discov* **2**, 401-404 (2012). https://doi.org/10.1158/2159-8290.CD-12-0095

62 Alexandrov, L. B. *et al.* Signatures of mutational processes in human cancer. *Nature* **500**, 415-421 (2013). https://doi.org/10.1038/nature12477

63 Hoek, K. S. & Goding, C. R. Cancer stem cells versus phenotype-switching in melanoma. *Pigment Cell Melanoma Res* **23**, 746-759 (2010). https://doi.org/10.1111/j.1755-148X.2010.00757.x

64 Cheng, P. F. *et al.* Methylation-dependent SOX9 expression mediates invasion in human melanoma cells and is a negative prognostic factor in advanced melanoma. *Genome Biol* **16**, 42 (2015). https://doi.org/10.1186/s13059-015-0594-4

65 Yang, X. *et al.* SOX9 is a dose-dependent metastatic fate determinant in melanoma. *J Exp Clin Cancer Res* **38**, 17 (2019). https://doi.org/10.1186/s13046-018-0998-6

66 Takahashi, M. *et al.* DrugMap: A quantitative pan-cancer analysis of cysteine ligandability. *Cell* **187**, 2536-2556 e2530 (2024). https://doi.org/10.1016/j.cell.2024.03.027

67 Hossain, S. M. & Eccles, M. R. Phenotype Switching and the Melanoma Microenvironment; Impact on Immunotherapy and Drug Resistance. *Int J Mol Sci* **24** (2023). https://doi.org/10.3390/ijms24021601

68 Travnickova, J. *et al.* Zebrafish MITF-Low Melanoma Subtype Models Reveal Transcriptional Subclusters and MITF-Independent Residual Disease. *Cancer Res* **79**, 5769-5784 (2019). https://doi.org/10.1158/0008-5472.CAN-19-0037

69 Weiss, J. M. *et al.* Shifting the focus of zebrafish toward a model of the tumor microenvironment. *Elife* **11** (2022). https://doi.org/10.7554/eLife.69703

70 Sun, N. *et al.* Development of drug-inducible CRISPR-Cas9 systems for large-scale functional screening. *BMC Genomics* **20**, 225 (2019). https://doi.org/10.1186/s12864-019-5601-9

71 Garraway, L. A. *et al.* Integrative genomic analyses identify MITF as a lineage survival oncogene amplified in malignant melanoma. *Nature* **436**, 117-122 (2005). https://doi.org/10.1038/nature03664

72 Huang, Y. *et al.* CRISPR-dCas13-tracing reveals transcriptional memory and limited mRNA export in developing zebrafish embryos. *Genome Biol* **24**, 15 (2023). https://doi.org/10.1186/s13059-023-02848-6

73 Kushawah, G. *et al.* CRISPR-Cas13d Induces Efficient mRNA Knockdown in Animal Embryos. *Dev Cell* **54**, 805-817 e807 (2020). https://doi.org/10.1016/j.devcel.2020.07.013

74 Jao, L. E., Wente, S. R. & Chen, W. Efficient multiplex biallelic zebrafish genome editing using a CRISPR nuclease system. *Proc Natl Acad Sci U S A* **110**, 13904-13909 (2013). https://doi.org/10.1073/pnas.1308335110

75 Ibarra-Garcia-Padilla, R., Howard, A. G. A. t., Singleton, E. W. & Uribe, R. A. A protocol for whole-mount immuno-coupled hybridization chain reaction (WICHCR) in zebrafish embryos and larvae. *STAR Protoc* **2**, 100709 (2021). https://doi.org/10.1016/j.xpro.2021.100709

76 Suresh, S. *et al.* Identifying the Transcriptional Drivers of Metastasis Embedded within Localized Melanoma. *Cancer Discov* **13**, 194-215 (2023). https://doi.org/10.1158/2159-8290.CD-22-0427

77 Labun, K. *et al.* CHOPCHOP v3: expanding the CRISPR web toolbox beyond genome editing. *Nucleic Acids Res* **47**, W171-W174 (2019). https://doi.org/10.1093/nar/gkz365

78 Clement, K. *et al.* CRISPResso2 provides accurate and rapid genome editing sequence analysis. *Nat Biotechnol* **37**, 224-226 (2019). https://doi.org/10.1038/s41587-019-0032-3

79 Lindsay, H. *et al.* CrispRVariants charts the mutation spectrum of genome engineering experiments. *Nat Biotechnol* **34**, 701-702 (2016). https://doi.org/10.1038/nbt.3628

80 Stirling, D. R. *et al.* CellProfiler 4: improvements in speed, utility and usability. *BMC Bioinformatics* **22**, 433 (2021). https://doi.org/10.1186/s12859-021-04344-9

81 Hao, Y. *et al.* Dictionary learning for integrative, multimodal and scalable single-cell analysis. *Nat Biotechnol* **42**, 293-304 (2024). https://doi.org/10.1038/s41587-023-01767-y

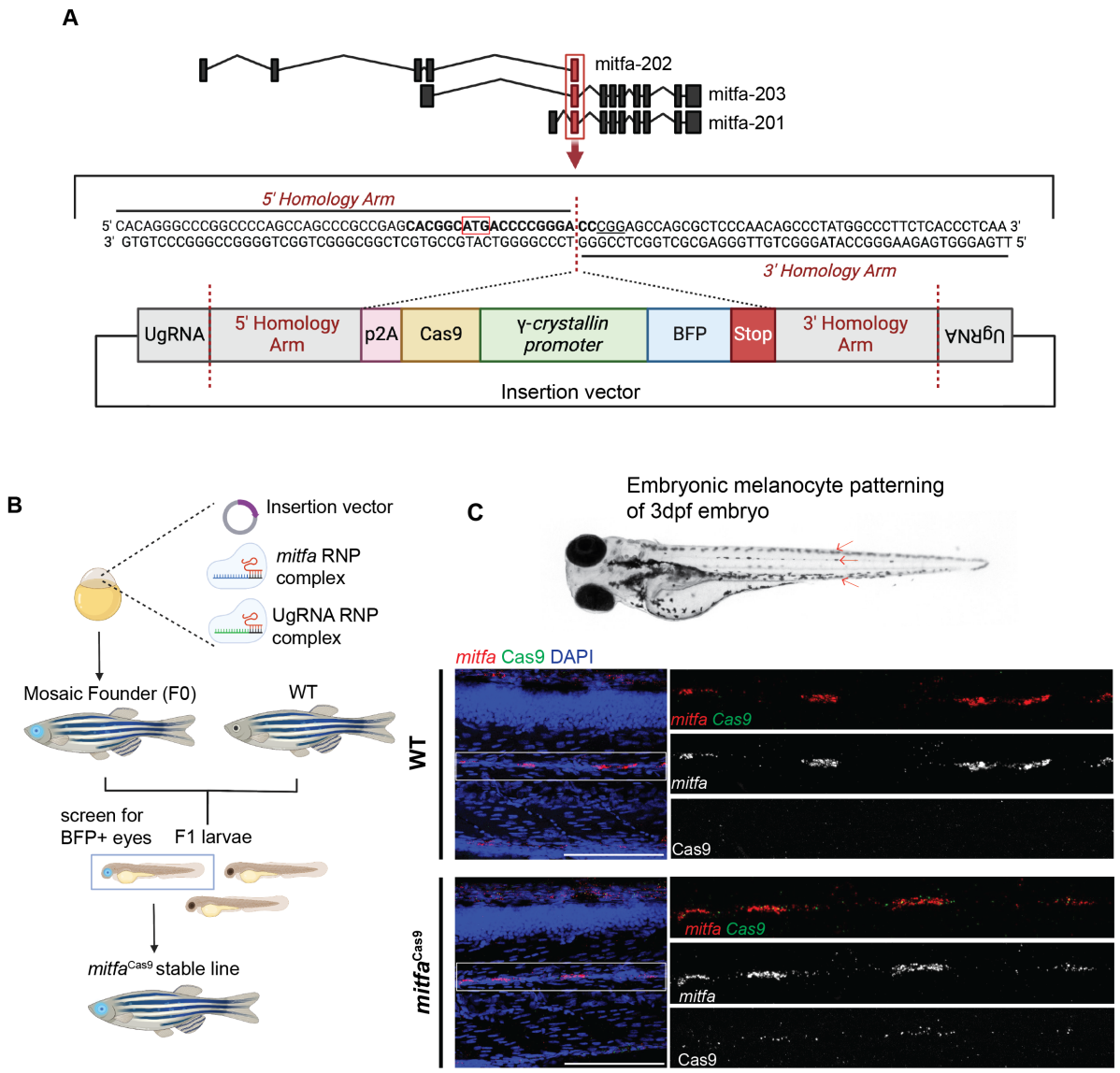

Figure 1. Targeted integration of Cas9 to the *mitfa* locus with GeneWeld knockin system. **(A)** Schematic depicting integration site and GeneWeld knock-in cassette. 5' and 3' homology arms are designed to target exon 2 of the zebrafish *mitfa* gene. The knock-in cassette includes p2A followed by Cas9 and BFP driven by the eye-specific promoter gamma-crystallin. **(B)** Pipeline to produce F1 mitfa^{Cas9} zebrafish. The GeneWeld knock-in vector and gRNAs targeting the *mitfa* genomic insertion site or specific sites on the knock-in vector (UgRNA) are co-injected into one-cell stage wild-type zebrafish embryos. Embryos are screened for BFP+ eyes marking mosaic integration. These mosaic founder fish are then raised to adulthood and crossed with wild-type fish. The resulting embryos are screened for BFP+ eyes and sequenced to confirm precise integration. **(C)** Fluorescent in situ hybridization chain reaction (FISH) on 3dpf wild-type and *mitfa*^{Cas9} embryos treated with 1-phenyl 2-thiourea (PTU). Arrows on the whole embryo image (WT 3dpf embryo not treated with PTU) indicate the embryonic melanocyte stripe regions where *mitfa* and Cas9 expression is expected. The presence of *mitfa* and Cas9 RNA was assessed by confocal microscopy at 40x magnification. Maximum intensity projections are shown. n=17 WT embryos and n=16 mitfa^{Cas9} embryos were screened. Scale bars, 100μm.

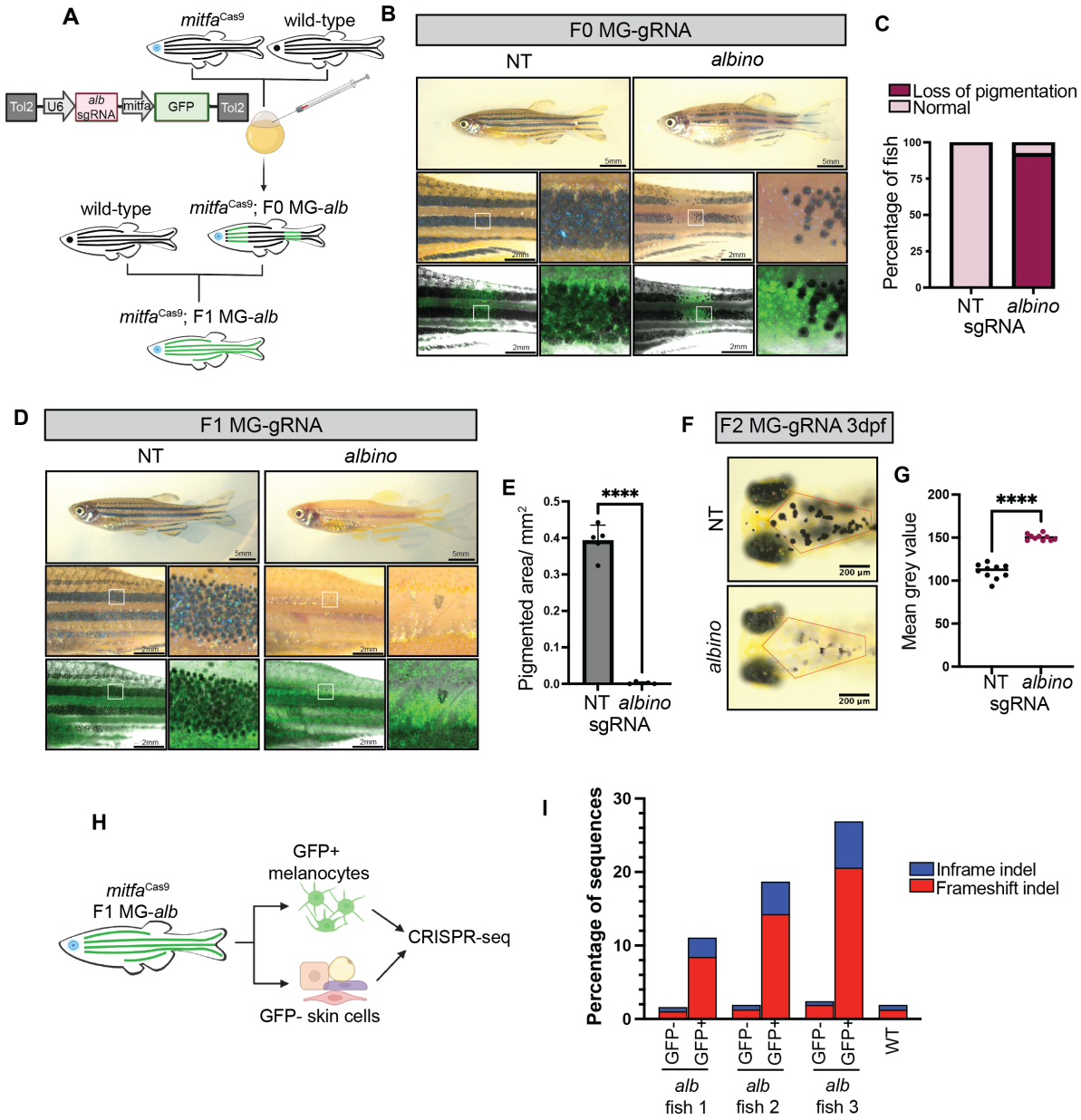

Figure 2. Melanocyte lineage-specific knockout of *albino* using *mitfa*^{Cas9} fish. **(A)** Pipeline to generate F0 and F1 U6:gRNA; *mitfa*:GFP (MG-gRNA) zebrafish. **(B)** Adult mitfa^{Cas9} MG-NT and MG-*albino* F0 fish. **(C)** Proportion of MG-NT (n=19) and MG-*albino* (n=25) F0 fish with loss of pigmentation phenotype. **(D)** Adult mitfa^{Cas9} MG-NT and MG-*albino* F1 fish. **(E)** Pigmented area/ mm^2 calculated for n=5 fish/ genotype within a defined rectangular region of interest (ROI) encompassing the top and middle melanocyte stripes. Two-sided student's *t*-test was used to assess statistical significance, **** $p < 0.0001$; error bars, SD. **(F)** 3dpf mitfa^{Cas9} MG-NT and MG-*albino* F2 fish. Representative embryos are shown for each genotype. **(G)** Mean grey value of head melanocytes calculated for n=10 embryos/genotype within a defined hexagonal ROI indicated as a red outline in 2F. Two-sided student's *t*-test was used to assess statistical significance, **** $p < 0.0001$. **(H)** Schematic for CRISPR sequencing protocol. **(I)** CRISPR-seq results are shown for WT and n=3 independent F1 MG-*albino* fish. Only GFP negative cells were isolated from WT fish. Results are shown as a fraction of sequences with indels calculated using CRISPRESSO.

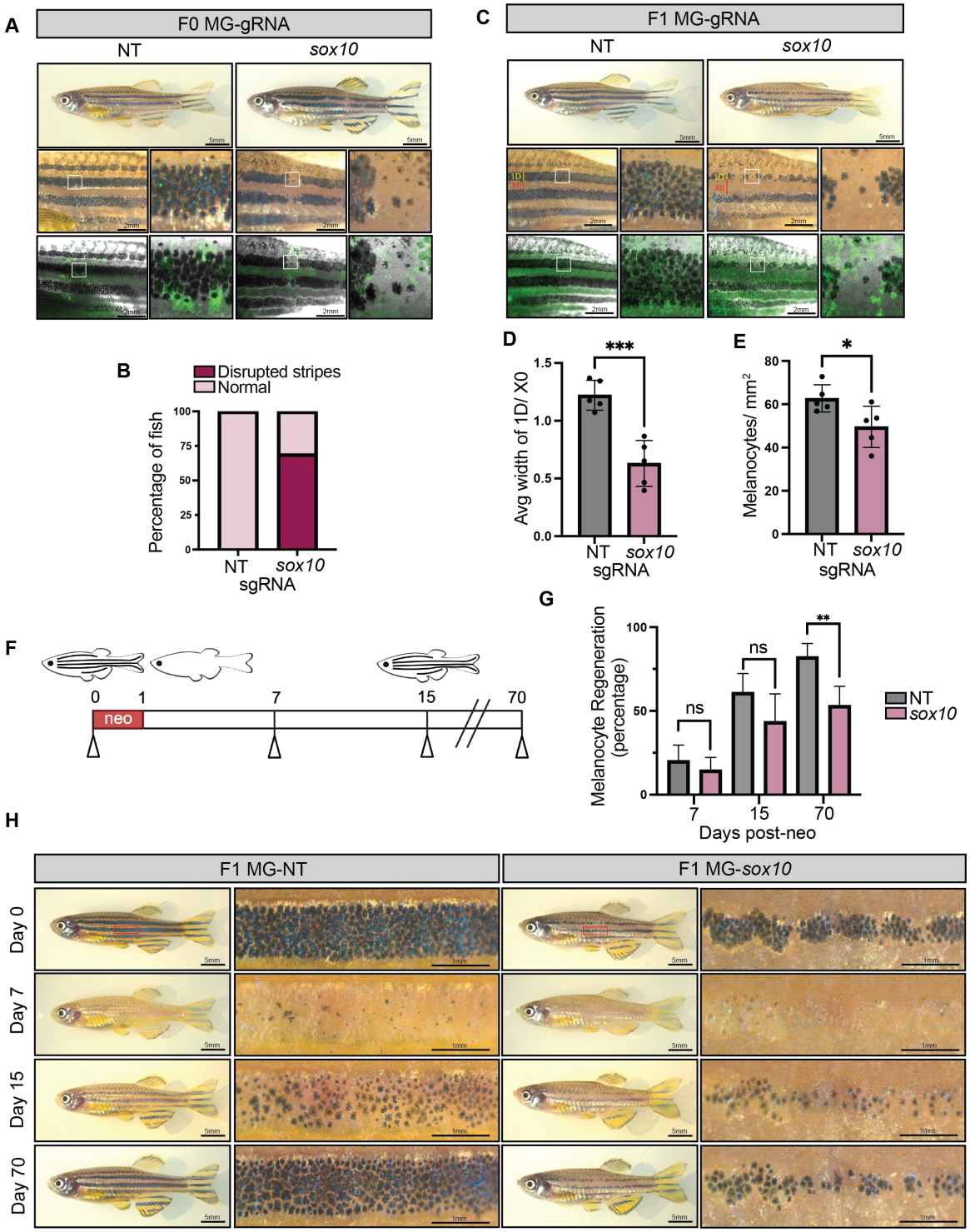

Figure 3. Melanocyte lineage-specific knockout of *sox10* using *mitfa*^{Cas9} fish. **(A)** Adult mitfa^{Cas9} MG-NT and MG-*sox10* F0 fish. **(B)** Proportion of MG-NT (n=19) and MG-*sox10* (n=16) F0 fish with disrupted stripes phenotype. **(C)** Adult mitfa^{Cas9} MG-NT and MG-*sox10* F1 fish. **(D)** The average width of melanocyte stripe 1D and xanthophore interstripe X0 was calculated for each fish by averaging 5 stripe/interstripe width measurements. N=5 fish per genotype. Two-sided student's *t*-test was used to assess statistical significance, *** $p < 0.001$;

error bars, SD. **(E)** F1 MG-NT (n=5) and MG-*sox10* (n=5) adult fish were treated with epinephrine and melanocytes were counted within a defined rectangular region of interest 3.46mm x 2.54mm encompassing the top and middle melanocyte stripes. Two-sided student's *t*-test was used to assess statistical significance, * $p < 0.05$; error bars, SD. **(F)** Schematic of neocuproine (neo) experimental setup. Adult mitfa^{Cas9} MG-NT (n= 5) and MG-*sox10* (n=5) F1 fish were treated with neocuproine for 24 hours to ablate melanocytes then imaged at day 7,15, and 70 to measure regeneration of melanocytes compared to day 0. **(G)** Quantification of melanocyte regeneration. Fish were treated with epinephrine prior to imaging to enable counting of melanocytes. Two-sided student's *t*-test was used to assess statistical significance, ** $p < 0.01$; error bars, SD. **(H)** Representative images are shown for MG-NT and MG-*sox10* fish pre- and post-neocuproine treatment.

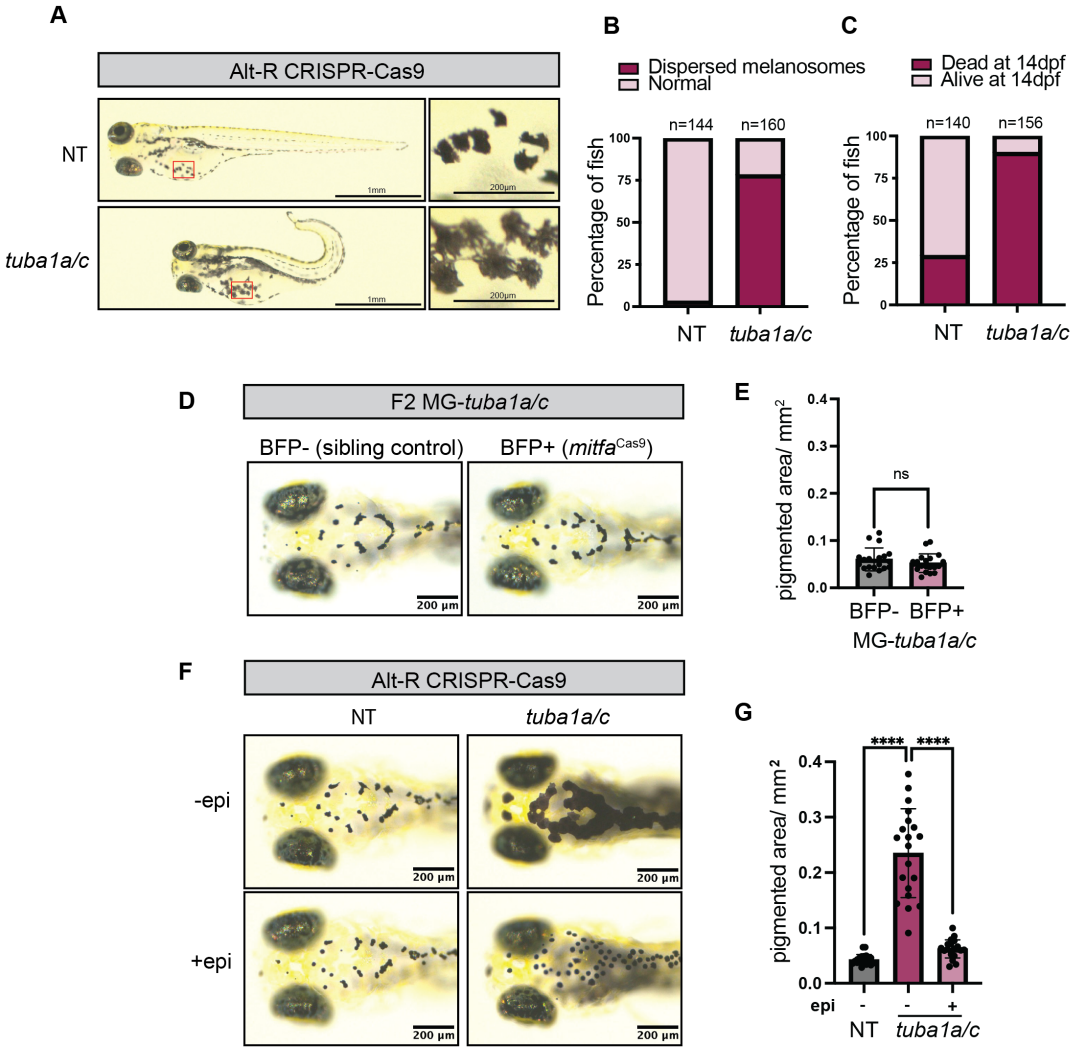

Figure 4. Non-autonomous function of *tuba1a/tuba1c* on melanocytes.
(A) 4dpf zebrafish embryos injected with either NT or *tuba1a/c* Alt-R CRISPR Cas9 gRNAs. **(B)** Percentage of NT or *tuba1a/c* Alt-R zebrafish embryos with dispersed melanocyte phenotypes. N=2 independent experiments. **(C)** Survival percentage is shown for NT and *tuba1a/c* Alt-R embryos. Embryos were counted at 24hpf and again at 14dpf to determine survival. **(D)** 4dpf mitfa^{Cas9} MG-*tuba1a/c* F2 embryos (BFP+ eyes) compared to sibling controls with no mitfa^{Cas9} (BFP- eyes). Representative embryos are shown for each genotype. **(E)** Pigmented area/ mm^2 calculated for n=19 embryos/genotype from two independent MG-*tuba1a/c* F2 clutches. Two-sided student's *t*-test was used to assess statistical significance, ns: no significance. **(F)** 4dpf Alt-R injected zebrafish embryos imaged before and after epinephrine (epi) treatment. **(G)** Pigmented area/ mm^2 calculated for n=20 embryos/genotype from two independent clutches. Two-sided student's *t*-test was used to assess statistical significance, **** $p < 0.0001$.

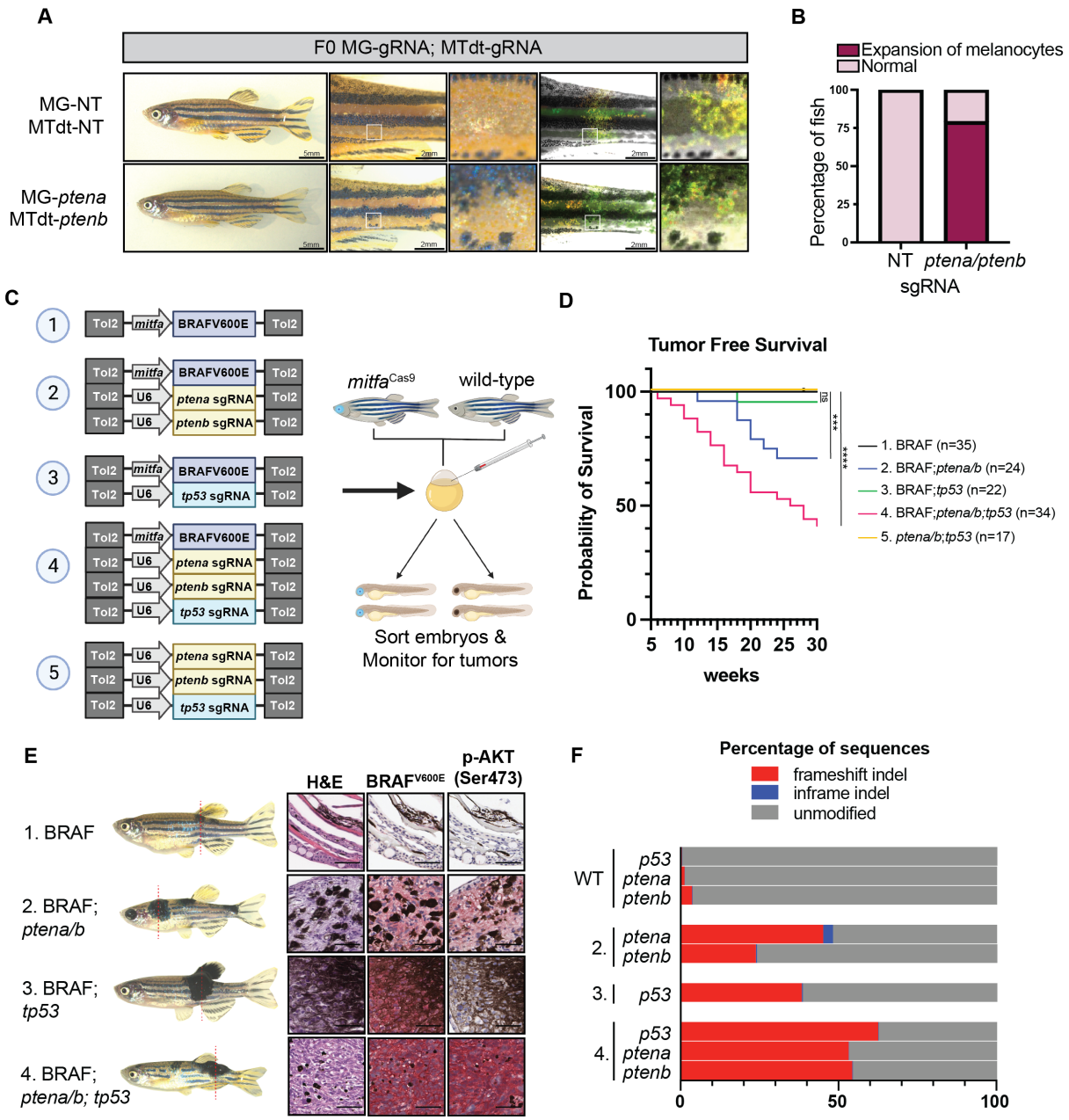

Figure 5. Generation of a zebrafish melanoma model in *mitfa*^{Cas9} fish.
(A) Adult mitfa^{Cas9} MG-NT; *mitfa*:TdTomato;U6:NT (MTdt-NT) and MG-*ptena*; *mitfa*:TdTomato;U6:*ptenb* (MTdT-*ptenb*) F0 fish. **(B)** Proportion of MG-NT; MTdT-NT (n=14) and MG-*ptena*; MTdT-*ptenb* (n=14) F0 fish with disrupted stripes phenotype. **(C)** Schematic of zebrafish tumorigenesis assay. Indicated plasmids are injected into one-cell stage embryos from crosses between mitfa^{Cas9} and WT fish. The mitfa:BRAF^{V600E} plasmid includes cardiac-specific cmlc2:GFP. Embryos were sorted for GFP+ hearts and BFP+ eyes and fish were screened every 2 weeks for tumors. **(D)** Tumor free survival curve. N=2 independent experiments. Tumors were tracked over the course of 30 weeks. Log-rank (Mantel-Cox) test was used to assess statistical significance, *** $p < 0.001$; **** $p < 0.0001$; ns: no significance. **(E)** Histology was performed on one fish from each indicated injection group. Dotted lines indicate site of sectioning. Red chromogen was used for all IHC staining. Scale bars, 50μm. **(F)** CRISPR-seq

results are shown for normal skin dissected from WT fish and tumors dissected from injection conditions 2, 3, and 4. Results are shown as a fraction of sequences with indels calculated using CRISPRESSO.

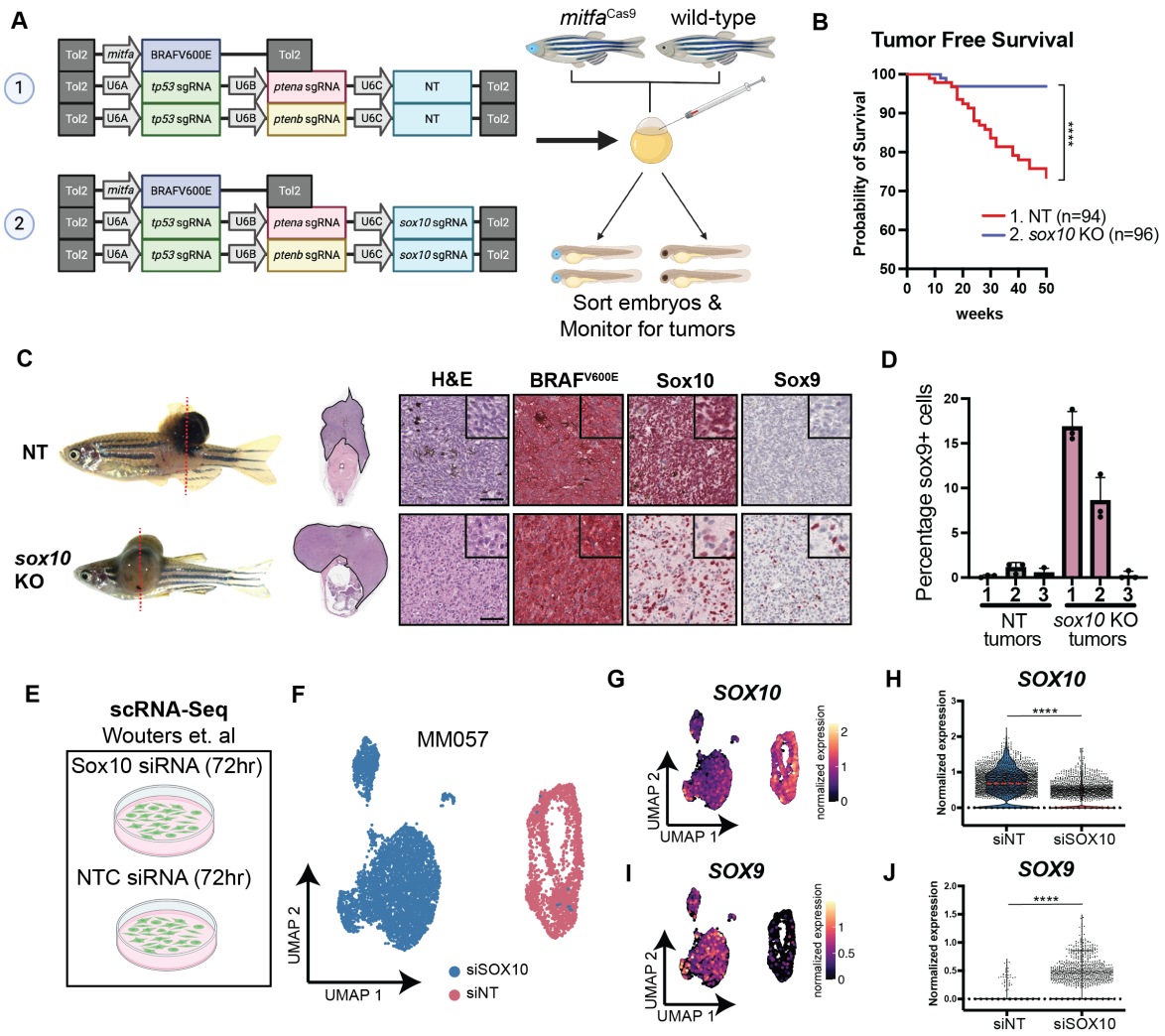

Figure 6. Melanoma specific knockout of *sox10* reduces tumor burden and induces phenotypic switching.

(A) Schematic of zebrafish tumorigenesis assay. Indicated plasmids are injected into one-cell stage embryos from crosses between mitfa^{Cas9} and WT fish. Embryos were sorted for GFP+ hearts and BFP+ eyes and fish were screened every 2 weeks for tumors. **(B)** Tumor free survival curve. N=3 independent experiments. Tumors were tracked over the course of 50 weeks. Log-rank (Mantel-Cox) test was used to assess statistical significance, **** $p < 0.0001$. **(C)** Histology is shown for one fish from each injection group. Dotted lines indicate site of sectioning. Red chromogen was used for all IHC staining. Scale bars, 50μm. **(D)** Color thresholding was used on IHC images to calculate the percentage of nuclei that stained positive for *sox9*. NT-1 n=1222 cells, NT-2 n=1620 cells, NT-3 n=2185 cells, sox10-1 n=970 cells, sox10-2 n=594, sox10-3 n=1046. Cells from n=3 images were analyzed for each tumor. **(E)** Schematic of scRNA-seq experimental setup from Wouters et al. Patient derived cell lines were treated with siRNAs targeting SOX10 or NTC and scRNA-seq was conducted at 72hrs. **(F)** UMAP of scRNA-seq dataset for MM057 cell line from Wouters et al. Cells from siSOX10 and siNT conditions are labeled. **(G)** Normalized expression of Sox10 per cell in UMAP space. **(H)** Violin plots of normalized expression of Sox10 per cell. Median is shown as dashed red line. Wilcoxon Rank Sum Test was used to assess statistical significance, **** $p < 0.0001$. **(I)** Normalized expression of Sox9 per cell in UMAP space. **(J)** Violin plots of normalized

expression of Sox9 per cell. Wilcoxon Rank Sum Test was used to assess statistical significance, **** $p < 0.0001$.

Figure S1

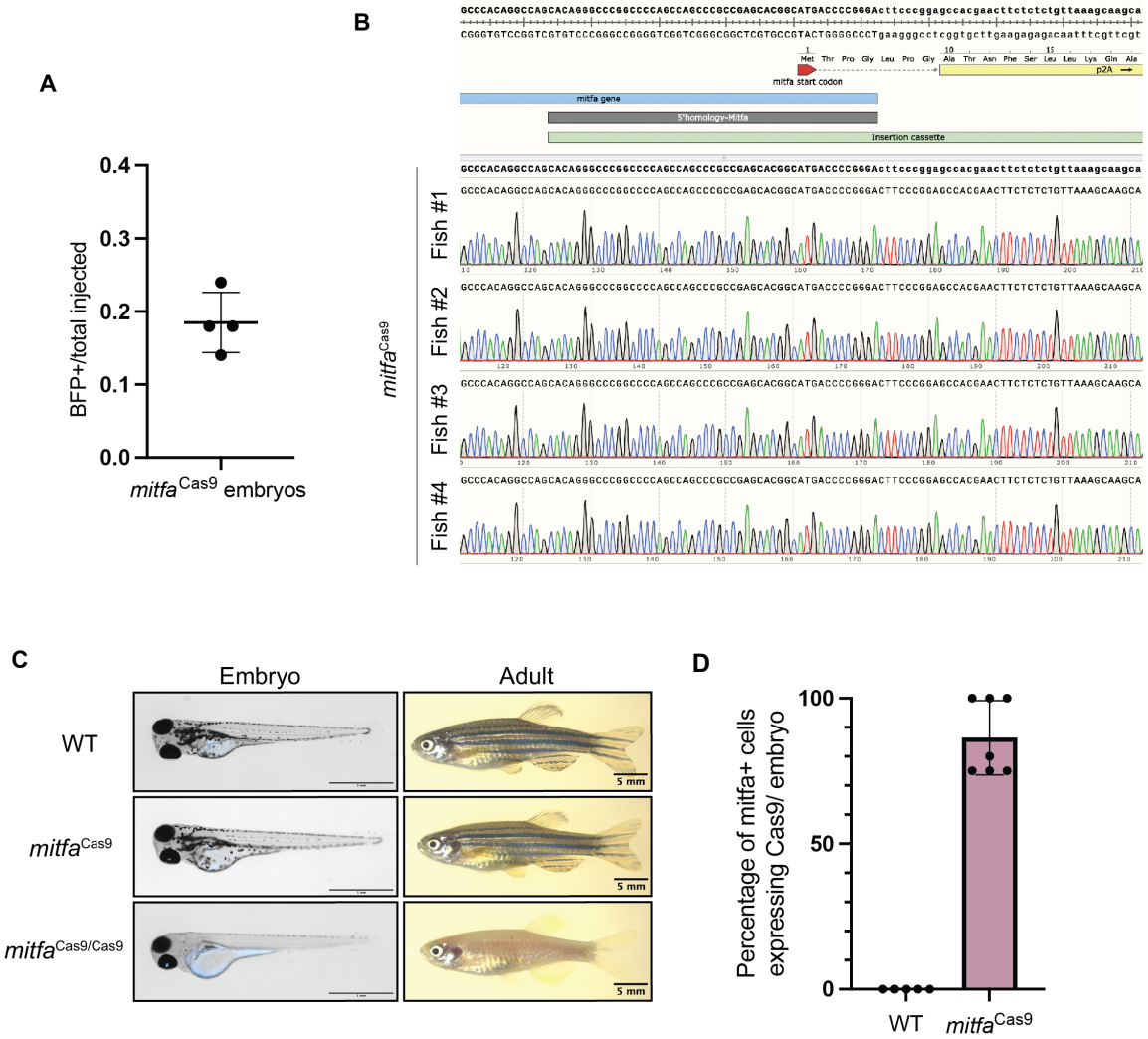

Figure S1. Validation of Cas9 knock-in.
(A) Integration efficiency of *mitfa*-targeted P2A-Cas9, gamma-cry:BFP vector. n= 4 independent experiments are shown with 50 embryos screened for each experiment. BFP+ eyes were detected in a total of 37/200 embryos. Error bars, SD. **(B)** Sanger sequencing results from four F1 fish with BFP+ eyes. Primers were designed with the forward primer located in the genomic *mitfa* locus and reverse primer within the Cas9 insertion cassette so that amplification can only occur if there is integration in the correct orientation. Snapgene was used to align sequences **(C)** Images of 3 day old and 3 month old clutchmates from a *mitfa*^{Cas9} incross. **(D)** Quantification of the percentage of *mitfa* positive cells that have Cas9 expression in each embryo. The presence of *mitfa* and Cas9 RNA was assessed by confocal microscopy from fluorescent in situ hybridization chain reaction (FISH) on 3dpf wild-type and *mitfa*^{Cas9} embryos. Out of 28 *mitfa*+ cells assessed across n=7 embryos, 24 had detectable Cas9 RNA.

Figure S2

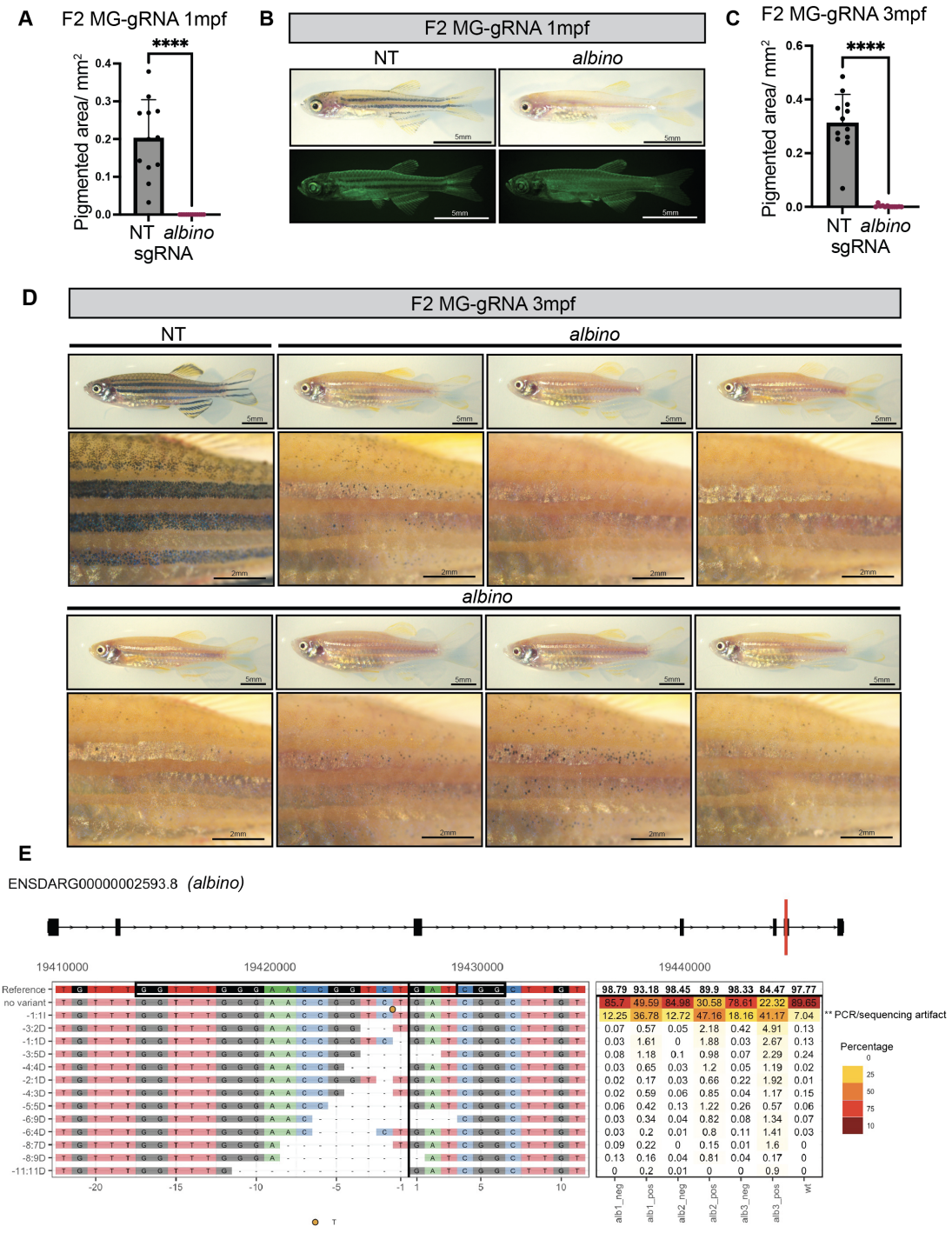

Figure S2. *albino* knockout fish.
(A) Quantification of pigmentation for 1mpf mitfa^{Cas9} MG-NT and MG-*albino* F2 fish. Pigmented area/ mm^2 calculated for n=12 fish/ genotype within a defined rectangular region of interest (ROI) encompassing the top and middle melanocyte stripes. Two-sided student's *t*-test was used to assess statistical significance, **** $p < 0.0001$; error bars, SD. **(B)** Color and GFP images of 1mpf mitfa^{Cas9} MG-NT and MG-*albino* F2 fish.

1212 **(C)** Pigmented area/ mm^2 calculated for n=12 fish/ genotype within a defined rectangular
1213 region of interest (ROI) encompassing the top and middle melanocyte stripes. Two-
1214 sided student's *t*-test was used to assess statistical significance, **** $p < 0.0001$; error
1215 bars, SD. **(D)** Color images of 3mpf mitfa^{Cas9} MG-NT and MG-*albino* F2 fish. **(E**) Indel
1216 chart for the *albino* locus produced using CRISPR Variants. **T insertion is observed
1217 across all samples, likely resulting from a PCR or sequencing artifact.
1218
1219
1220

Figure S3

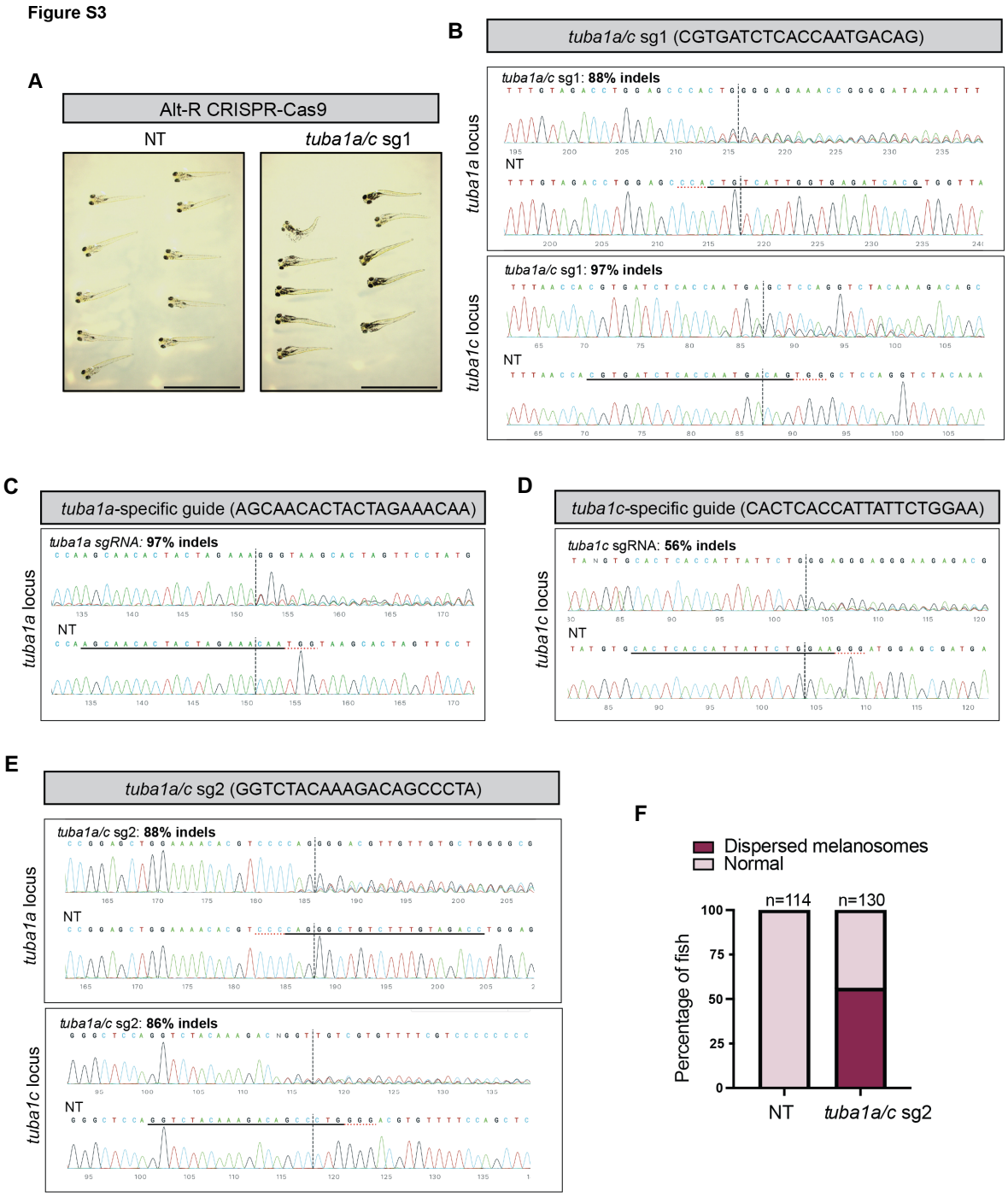

1221

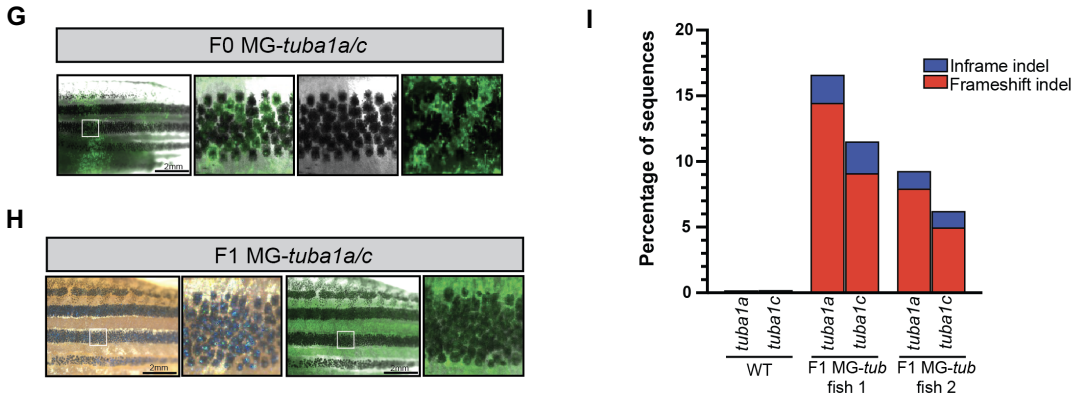

Figure S3. Knockout of *tuba1a*

(A) 6dpf zebrafish embryos injected with either NT or *tuba1a/c* sg1 Alt-R CRISPR Cas9 gRNAs. **(B)** Validation of Alt-R CRISPR Cas9 *tuba1a/c* sg1 targeting with sanger sequencing. Synthego Ice software estimated 88% indels in the *tuba1a* locus and 97% indels in the *tuba1c* locus. **(C)** Validation of Alt-R CRISPR Cas9 *tuba1a*-specific sgRNA targeting with sanger sequencing. Synthego Ice software estimated 97% indels in the *tuba1a* locus. **(D)** Validation of Alt-R CRISPR Cas9 *tuba1c*-specific sgRNA targeting with sanger sequencing. Synthego Ice software estimated 56% indels in the *tuba1c* locus.**(E)** Validation of Alt-R CRISPR Cas9 *tuba1a/c* sg2 targeting with sanger sequencing. Synthego Ice software estimated 88% indels in the *tuba1a* locus and 86% indels in the *tuba1c* locus. **(F)** Percentage of NT or *tuba1a/c* sg2 Alt-R zebrafish embryos with dispersed melanocyte phenotypes. N=2 independent experiments. **(G)** Adult mitfa^{Cas9} MG-*tuba1a/c* F0 fish. Image is representative of n=7 F0 fish. **(H)** Adult mitfa^{Cas9} MG-*tuba1a/c* F1 fish. Image is representative of n=14 F1 fish. **(I)** CRISPR-seq results are shown for WT and n=2 F1 MG-*tuba1a/c* fish sorted for GFP+ cells. Results are shown as a fraction of sequences with indels calculated using CRISPRESSO.

Figure S4

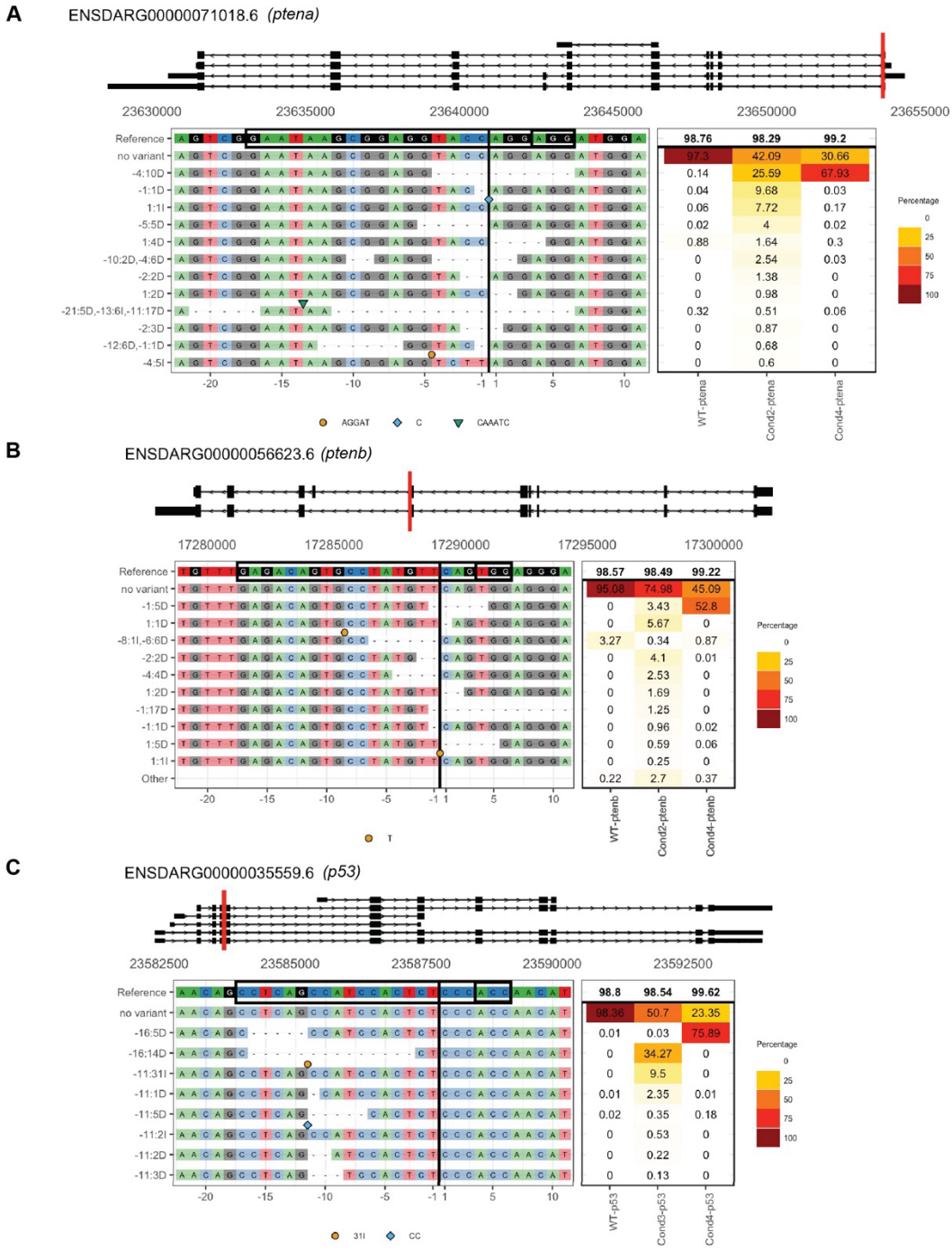

Figure S4. CRISPR-seq for tumor suppressor genes.
(**A**) Indel chart for the *ptena* locus produced using CRISPRVariants. (**B**) Indel chart for the *ptenb* locus produced using CRISPRVariants. (**C**) Indel chart for the *p53* locus produced using CRISPRVariants.

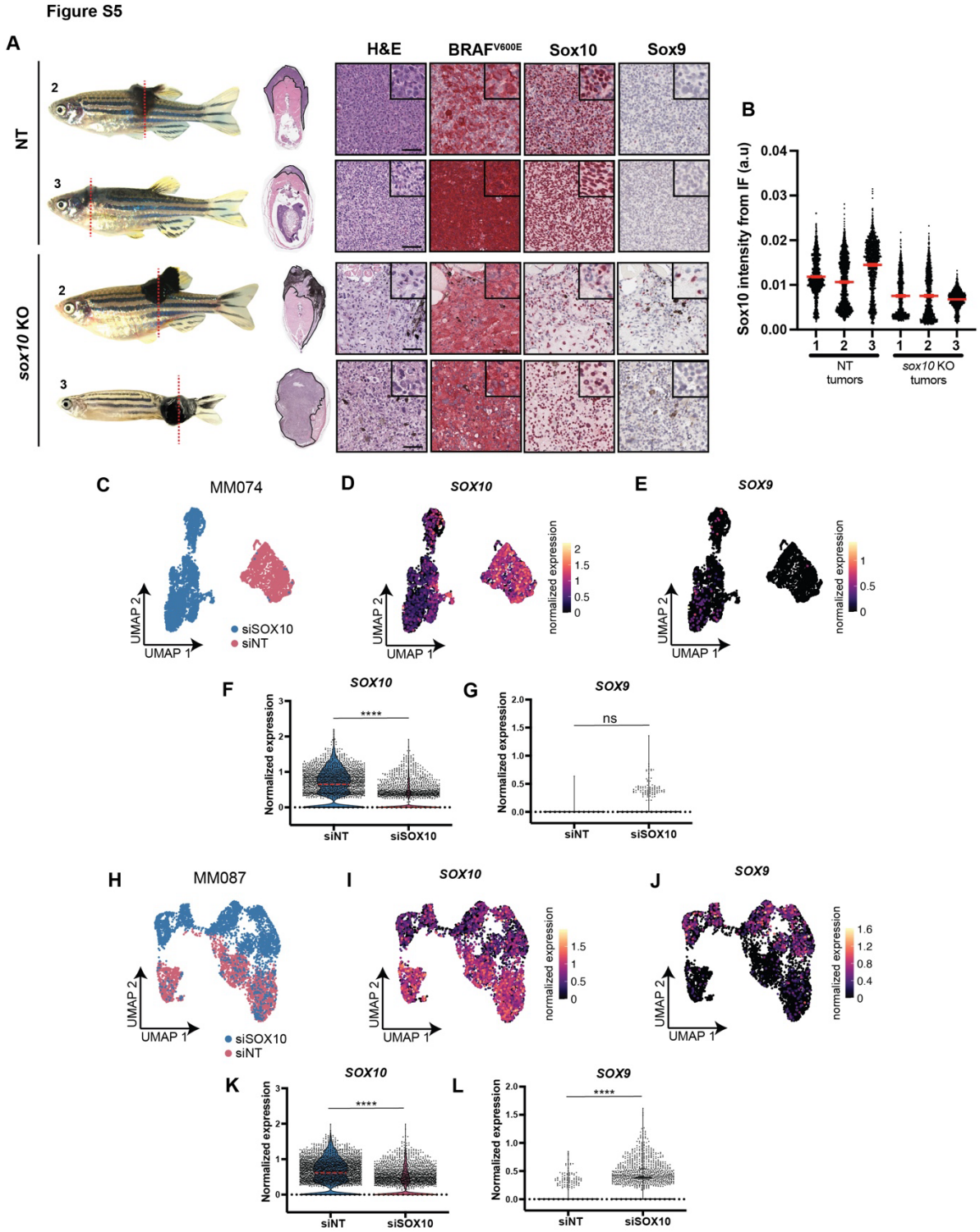

Figure S5. *In vivo* and *in vitro* targeting of Sox10 leads to upregulation of Sox9. (**A**) Histology is shown for two additional fish from each injection group. Dotted lines indicate site of sectioning. Red chromogen was used for all IHC staining. Scale bars, 50µm. (**B**) *Sox10* intensity per nucleus from NT and *sox10* KO tumors. Intensity was calculated from immunofluorescence staining of *Sox10*. Red lines indicate mean with

95% CI. Each point represents one nuclei. NT-1 n=1334 cells, NT-2 n=1606 cells, NT-3 n=1204 cells, sox10-1 n=869 cells, sox10-2 n=998, sox10-3 n=1046. Cells from n=3 images were analyzed for each tumor. **(C**) UMAP of scRNA-seq dataset for MM074 cell line from Wouters et al. Cells from siSOX10 and siNT conditions are labeled. **(D**) Normalized expression of SOX10 per cell in UMAP space in MM074 cell line. **(E**) Normalized expression of SOX9 per cell in UMAP space in MM074 cell line. **(F**) Violin plots of normalized expression of SOX10 per cell. Median is shown as dashed red line. Wilcoxon Rank Sum Test was used to assess statistical significance, **** $p < 0.0001$. **(G**) Violin plots of normalized expression of SOX9 per cell. Wilcoxon Rank Sum Test was used to assess statistical significance; ns: no significance. **(H**) UMAP of scRNA-seq dataset for MM087 cell line from Wouters et al. Cells from siSOX10 and siNT conditions are labeled. **(I**) Normalized expression of SOX10 per cell in UMAP space in MM087 cell line. **(J**) Normalized expression of SOX9 per cell in UMAP space in MM087 cell line. **(K**) Violin plots of normalized expression of SOX10 per cell. Median is shown as dashed red line. Wilcoxon Rank Sum Test was used to assess statistical significance, **** $p < 0.0001$. **(L**) Violin plots of normalized expression of SOX9 per cell. Wilcoxon Rank Sum Test was used to assess statistical significance, **** $p < 0.0001$.